Scientific Research Publishing

Open Journal of Applied Sciences, 2025, 15(3), 638-669
https://www.scirp.org/journal/ojapps
ISSN Online: 2165-3925
ISSN Print: 2165-3917

Optimization of Anti-Resonance Peaks for Time-Delay Coupled Dynamic Vibration Absorbers with Inertial Containment

Hao Wu, Yanying Zhao, Weikai Wang, Xiangzhi Xiao

School of Aircraft Engineering, Nanchang Hangkong University, Nanchang, China
Email: 1101231706@qq.com

How to cite this paper: Wu, H., Zhao, Y.Y., Wang, W.K. and Xiao, X.Z. (2025) Optimization of Anti-Resonance Peaks for Time-Delay Coupled Dynamic Vibration Absorbers with Inertial Containment. *Open Journal of Applied Sciences*, **15**, 638-669.
https://doi.org/10.4236/ojapps.2025.153042

Received: February 27, 2025
Accepted: March 17, 2025
Published: March 20, 2025

Abstract

In this paper, a time delay is coupled to a dynamic vibration absorber with an inerter-based grounded stiffness that contains an amplification mechanism, and a model of the dynamic vibration absorber with time-delay feedback control containing an inerter is obtained. For this model, the vibration differential equation of the system is first established, and the optimal structural parameters of the passive system with an inerter are analyzed under the condition of no time delay. When the time delay is considered, the characteristic equation of the system is a transcendental equation with exponential terms. The CTCR method and the Dixon resultant are used to analyze the stability of the system, and the stable intervals of the feedback gain coefficient and time delay are obtained. Then, according to the anti-resonance peak optimization criteria, the structural parameters of the system are further adjusted under the condition of ensuring the system's stability, and a set of optimal structural parameters is successfully obtained, which can not only meet the minimum anti-resonance peak criterion but also have a wider vibration reduction frequency band and a good vibration reduction effect. Finally, the optimization results are verified in both the time domain and the frequency domain. Compared with the traditional dynamic vibration absorber, the dynamic vibration absorber designed in this paper has achieved a good vibration reduction effect.

Keywords

Inerter, Time-Delay, Dnamic Vibration Absorber, Anti-Resonance Peak Optimization

1. Introduction

A dynamic vibration absorber is a mechanical device used to reduce vibrations,

mainly by interacting with the main system to absorb or counteract part of the vibration energy. The Danish engineer Frahm [1] invented a non-damped dynamic vibration absorber. When the external excitation frequency of the main system is close to its natural frequency, the vibration absorber has a good vibration reduction effect, but the vibration-reduction frequency band is narrow. Ormondroyd [2] first added damping to the DVA and proposed the fixed-point theory. Den Hartog [3] [4] further optimized and improved the fixed-point theory and proposed the Voigt-type dynamic vibration absorber with a wider vibration reduction frequency band and better vibration reduction effect. Based on the dynamic vibration absorber studied by Den Hartog, Brock [5] proposed a damping optimization formula. Nishihara *et al.* [6] and Asami *et al.* [7] used the fixed-point theory to optimize the design of the damped dynamic vibration absorber and obtained the analytical expressions of the optimal structural parameters. Aiming at the problems of narrow vibration reduction frequency band and poor vibration reduction effect of linear dynamic vibration absorbers, scholars began to study non-linear dynamic vibration absorbers. Liu Lilan *et al.* [8] designed a bistable dynamic vibration absorber with non-linear damping, which has a better vibration reduction effect than the traditional linear bistable vibration absorber. Zhao Yanying *et al.* [9] [10] studied the dynamic vibration absorber with time delay non-linearity, reduced the vibration of the main system by adjusting the feedback gain coefficient and the time delay, and verified the accuracy of the results through numerical simulation.

With the continuous improvement of the requirements for vibration reduction, new components and technologies have been gradually introduced into the design of vibration reduction systems and achieved remarkable results. Components such as negative stiffness and dampers, such as emerging technologies, can significantly improve the performance of vibration absorbers. Peng Haibo *et al.* [11] proposed a new dynamic vibration absorber model containing a negative stiffness spring element, obtained the analytical solution of the system through the Laplace transform, and used the fixed point theory to obtain the optimal damping ratio and frequency ratio of the system. Oyelad *et al.* [12] used two mutually repulsive magnets to generate a negative magnetic spring (NMS). It was found that the dynamic equations of the system containing the NMS spring can be derived using Hamilton's principle. Yi Ju *et al.* [13] proposed a tuned negative stiffness inerter mass damper (TNIMD). After obtaining the coupling equations of the system through the Lagrange equation, the negative stiffness coefficient was optimized using the fixed-point theory. Gao Hui *et al.* [14] combined the vibration reduction advantages of negative stiffness and tuned viscous dampers, studied the vibration reduction performance of the tuned negative—stiffness—inerter mass damper (TNSIMD), and found that TNSIMD can give full play to its tuning function and negative stiffness advantage, significantly improving the vibration reduction effect of the system. Wang Jue *et al.* [15] proposed three inerter based vibration reduction systems with negative stiffness (N-ISD) and derived the analytical solutions

of the system parameters using the H∞ and H2 optimization criteria. Zhang Yin *et al.* [16] established a numerical model of a negative stiffness damper under flexible support with reference to a cable stayed bridge, verified the model and identified the additional damping ratio. The research results show that the established numerical model of the support negative stiffness damper is in good agreement with the experimental results and can accurately predict the dynamic behavior of the system. Tu *et al.* [17] introduced a negative stiffness magnetic spring into the automotive suspension system and conducted experimental research using specially arranged cylindrical magnets. The results show that the negative stiffness magnetic spring has a good vibration reduction effect on non-linear systems. Benacchio *et al.* [18] used magnets to build a variable stiffness dynamic vibration absorber (MVA). Under the condition of containing negative stiffness elements, the parameters of the MVA can be adjusted to design a non-linear vibration absorber or a bistable absorber with negative linear stiffness. Hu Fangyuan *et al.* [19] proposed a time domain non-parametric identification method based on the restoring force surface aiming at the difficult problem of identifying the restoring force of the negative stiffness non-linear oscillator. The results show that using the restoring force surface method to identify the negative stiffness non-linear oscillator can achieve a good vibration-reduction effect.

The amplification mechanism is a device that amplifies the input force or displacement through structural design to improve the performance of the system. Among them, amplification mechanisms such as levers and inerters have good effects in the field of vibration control and are widely used. Zhang *et al.* [20] introduced a lever to reduce the overall mass of the device and proposed a new non-linear energy sink. When the lever fulcrum is in the optimal position, the lever-type non-linear energy sink is superior to the traditional non-linear dynamic vibration absorber in vibration reduction performance. Yang Weiqing *et al.* [21] carried out the vibration-reduction design and experimental research based on the lever-type tuned mass damper for the wind-induced vibration problem of long double-cable slings, and designed the lever-type tuned mass damper according to the optimal parameters. Xu Ximing *et al.* [22] proposed a structural scheme of the lever—type vibration—reduction device for the bogie of a heavy load truck aiming at the problems of complex structure and unstable vibration reduction performance of the shock absorber of a certain type of truck bogie and elaborated the structural principle of the vibration reduction device in detail. Li Chunxiang *et al.* [23] studied the dynamic characteristics of the lever—type tuned mass damper and found that this mechanism has a better tuning frequency ratio and a smaller optimal damping ratio than the traditional TMD. Wang *et al.* [24] proposed a dynamic vibration absorber with inerter negative stiffness coupling (INDVAs). Compared with the traditional DVA, INDVAs have a wider vibration reduction frequency band and better vibration reduction performance. Chen Jie *et al.* [24] designed two new negative stiffness dynamic vibration absorber structures containing inerters and obtained the analytical expressions of their optimal parame-

ters. It was found that the dynamic vibration absorber based on inerter negative stiffness is more effective than the traditional dynamic vibration absorber in the vibration control problem of beams.

The amplification mechanism has excellent performance in the field of vibration control. In this paper, a new dynamic vibration absorber with an amplification mechanism proposed in reference [25] is taken as the research object. This model combines the dual advantages of the inerter and the amplification mechanism, not only showing excellent vibration-reduction effects but also having certain flexibility and economy in structural design and material use. Aiming at the problems of a narrow vibration reduction frequency band and the sensitivity of the amplitude of the main system to the change of the excitation frequency near the anti-resonance frequency in the passive-controlled two-degree-of-freedom system, time-delay feedback active control is introduced, and a new optimization design method is proposed. Through the optimization program, the optimal parameter configuration that satisfies the minimum anti-resonance peak criterion and has a good vibration-reduction effect is successfully obtained, and its feasibility and superiority in practical applications are proved through numerical simulation and comparative analysis.

2. Mechanical Model and Vibration Differential Equation

2.1. Modeling and Dynamic Equations of the Vibration System with Time-Delay

For the two degrees of freedom system with an amplification mechanism, the effect of vibration control using passive vibration reduction methods is extremely limited. To further widen its vibration reduction frequency band, time delay feedback control is considered based on reference [25]. The mechanical model of time delay feedback control is shown in **Figure 1**. There is a lever with fixed support between the main system and the dynamic vibration absorber. The main system and the vibration absorber are connected via sliders at both ends of the lever, forming a complete system. Here, r_1 and r_2 respectively represent the distances from the lever support point O to the fixed points M and N of the sliders. m_1, c_1, and k_1 respectively represent the mass, damping, and stiffness of the main system; m_2, c_2, and k_2 respectively represent the mass, damping, and stiffness of the vibration absorber; k represents the grounded stiffness; x_1 and x_2 respectively represent the displacements of the main system and the vibration absorber; τ, g_1 respectively represent the time delay and the feedback gain coefficient; b represents the inerter; F_0, ω respectively represent the amplitude and frequency of the external excitation. Assume that $L = r_1/r_2$ is the amplification ratio of the system. According to the similarity theorem of triangles, the force acting on the main system is L times that on the vibration absorber, and the displacement is $1/L$ of the vibration absorber.

Give the vibration differential equations of the system according to Newton's second law:

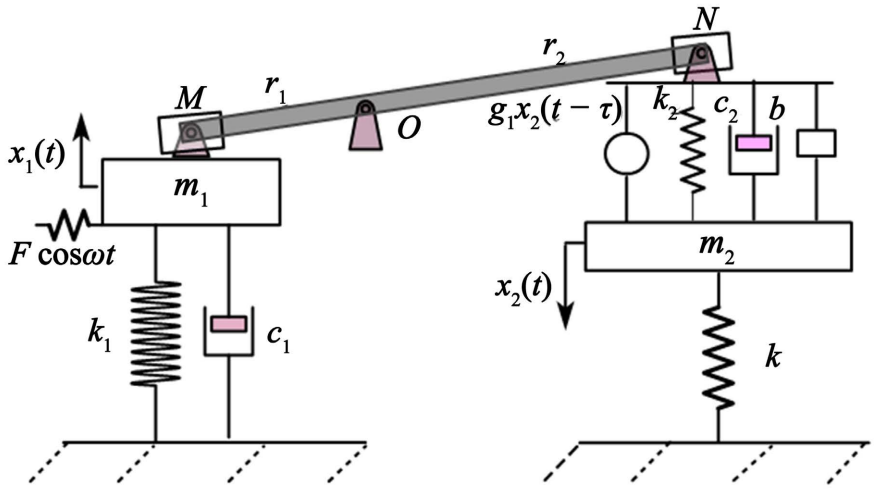

Figure 1. Mechanical model of the time delay dynamic vibration absorber with an amplification mechanism.

$$\begin{cases} m_1\ddot{x}_1 + k_2L\left(Lx_1 - x_2\right) + c_1\dot{x}_1 + k_1x_1 + c_2L\left(L\dot{x}_1 - \dot{x}_2\right) \\ \quad - g_1Lx_2\left(t-\tau\right) + bL\left(L\ddot{x}_1 - \ddot{x}_2\right) = F_0\cos\left(\omega t\right) \\ m_2\ddot{x}_2 - b\left(L\ddot{x}_1 - \ddot{x}_2\right) - c_2\left(L\dot{x}_1 - \dot{x}_2\right) - k_2\left(Lx_1 - x_2\right) + g_1x_2\left(t-\tau\right) + kx_2 = 0 \end{cases} \tag{1}$$

In order to simplify the calculation process, the following dimensionless quantities are introduced:

$$\begin{gathered} \omega_1 = \sqrt{\frac{k_1}{m_1}}, \omega_2 = \sqrt{\frac{k_2}{m_2}}, \mu = \frac{m_2}{m_1}, \xi_1 = \frac{c_1}{2m_1\omega_1}, \xi_2 = \frac{c_2}{2m_2\omega_2}, p = \frac{\omega_2}{\omega_1}, \\ \Omega = \frac{\omega}{\omega_1}, g = \frac{g_1}{k_2}, \tilde{x}_1 = \frac{k_1x_1}{F_0}, \tilde{x}_2 = \frac{k_1x_2}{F_0}, \tilde{t} = \omega_1t, \tilde{\tau} = \omega_1\tau, \beta = \frac{b}{m_2}, \alpha = \frac{k}{k_2}, \end{gathered} \tag{2}$$

For the convenience of writing, the above parameters are expressed as: $x_1 = \tilde{x}_1$, $x_2 = \tilde{x}_2, t = \tilde{t}, \tau = \tilde{\tau}$, where $(\cdot)' = \mathrm{d}(\cdot)/\mathrm{d}t, (\cdot)'' = \mathrm{d}^2(\cdot)/\mathrm{d}t^2$. Substitute the above dimensionless quantities, and transform Equation (1) into the following dimensionless form:

$$\begin{cases} x_1'' + \left(1 + \mu L^2p^2\right)x_1 + 2\left(\xi_1 + L^2\mu p\xi_2\right)x_1' - L\mu p^2x_2 - 2L\mu p\xi_2x_2' \\ \quad + \beta\mu L\left(L\ddot{x}_1 - \ddot{x}_2\right) - Lp^2\mu gx_2\left(t-\tau\right) = \cos\left(\Omega t\right) \\ x_2'' + \left(1+\alpha\right)p^2x_2 + 2p\xi_2x_2' - Lp^2x_1 - 2Lp\xi_2x_1' - \beta\left(L\ddot{x}_1 - \ddot{x}_2\right) + gp^2x_2\left(t-\tau\right) = 0 \end{cases} \tag{3}$$

Assume that the solution of (3) is as follows:

$$\begin{bmatrix} x_1 \\ x_2 \end{bmatrix} = \begin{bmatrix} \overline{x}_1 \\ \overline{x}_2 \end{bmatrix} \mathrm{e}^{j\Omega t} \tag{4}$$

In the formula, j is the imaginary unit. Substitute Equation (4) into Equation (3), and the expression of its analytical solution is obtained as follows:

$$\begin{bmatrix} \overline{x}_1 \\ \overline{x}_2 \end{bmatrix} = \frac{1}{\Delta(\Omega)} \begin{bmatrix} -\Omega^2 + 2p\xi_2j\Omega + \left(1+\alpha\right)p^2 + p^2g\mathrm{e}^{-j\Omega\tau} - \beta\Omega^2 \\ 2Lp\xi_2j\Omega + Lp^2 - \beta L\Omega^2 \end{bmatrix} \tag{5}$$

$$\begin{aligned}\Delta(\Omega)=&\left(-\Omega^2+1+L^2p^2\mu+2\xi_1 j\Omega+2L^2\mu p\xi_2 j\Omega-\beta\mu L^2\Omega^2\right)\\&\times\left(-\Omega^2+2p\xi_2 j\Omega+(1+\alpha)p^2+p^2 g\mathrm{e}^{-j\Omega\tau}-\beta\Omega^2\right)\\&-\left(2L\mu p\xi_2 j\Omega+Lp^2\mu+L\mu p^2 g\mathrm{e}^{-j\Omega\tau}-\beta\mu L\Omega^2\right)\\&\times\left(2Lp\xi_2 j\Omega+Lp^2-\beta L\Omega^2\right)\end{aligned}\tag{6}$$

Separate the expressions of $\bar{x}_1$ and $\bar{x}_2$ into real and imaginary parts and find their moduli. Define the expressions of the variables A_1 and A_2 as follows:

$$A_i=\left\|x_i\right\|_{(i=1,2)}\tag{7}$$

where, $\bar{x}_1$ and $\bar{x}_2$ represent the amplitude amplification factors of the main system and the vibration absorber respectively.

2.2. Analysis of Passive Vibration Reduction System's Structural Parameters

For the above time-delay vibration reduction system, if it is assumed that the damping of the main system $\xi_1=0$, and the time-delay feedback gain coefficient $g=0$, then the above system will degenerate into a passive dynamic vibration absorber. Substitute the above system parameters into Equation (3), and the motion differential equation of the passive vibration reduction device is obtained as follows:

$$\begin{cases}x_1''+\left(1+\mu L^2p^2\right)x_1+2L^2\mu p\xi_2 x_1'-L\mu p^2x_2-2L\mu p\xi_2 x_2'+\beta\mu L\left(L\ddot{x}_1-\ddot{x}_2\right)=\cos(\Omega t)\\x_2''+(1+\alpha)p^2x_2+2p\xi_2 x_2'-Lp^2x_1-2Lp\xi_2 x_1'-\beta\left(L\ddot{x}_1-\ddot{x}_2\right)=0\end{cases}\tag{8}$$

Similarly, assume that the form of the solution of the equation is as shown in Equation (4). After substitution, the form of the solution of the passive vibration reduction device is obtained as follows:

$$\begin{bmatrix}\bar{x}_1\\\bar{x}_2\end{bmatrix}=\frac{1}{\Delta(\Omega)}\begin{bmatrix}-\Omega^2+2p\xi_2 j\Omega+(1+\alpha)p^2-\beta\Omega^2\\2Lp\xi_2 j\Omega+Lp^2-\beta L\Omega^2\end{bmatrix}\tag{9}$$

$$\begin{aligned}\Delta(\Omega)=&\left(-\Omega^2+1+L^2p^2\mu+2L^2\mu p\xi_2 j\Omega-\beta\mu L^2\Omega^2\right)\\&\times\left(-\Omega^2+2p\xi_2 j\Omega+(1+\alpha)p^2-\beta\Omega^2\right)\\&-\left(2L\mu p\xi_2 j\Omega+Lp^2\mu-\beta\mu L\Omega^2\right)\left(2Lp\xi_2 j\Omega+Lp^2-\beta L\Omega^2\right)\end{aligned}\tag{10}$$

Separate the real and imaginary parts of the above expression and calculate its modulus. The expression for the amplitude amplification factor A_1 of the passive vibration reduction system is obtained as follows:

$$A_1=\left\|x_1\right\|=\sqrt{\frac{C^2+D^2}{A^2+B^2}}\tag{11}$$

In the formula:

$$\begin{cases}A=2p\Omega\xi_2\left[1+L^2\mu\alpha p^2-\Omega^2\left(1+L^2\mu\right)\right]\\B=\left(1-\Omega^2\right)\left[(1+\beta)\Omega^2-(1+\alpha)p^2\right]-L^2\beta\mu\Omega^4-L^2\mu p^2\left[\alpha p^2-(1+\alpha\beta)\Omega^2\right]\\C=-\Omega^2+(1+\alpha)p^2-\beta\Omega^2\\D=2p\xi_2\Omega\end{cases}\tag{12}$$

For the PDVA system with the main system having no damping, through the fixed point theory, it is easy to prove that the normalized amplitude-frequency response curves will all pass through two points that are independent of the damping ratio. Figure 2 shows the normalized curves when the damping ratios ξ_2 are 0.3, 0.5, and 0.7 respectively. It can be seen from the figure that the three curves all intersect at point P and point Q.

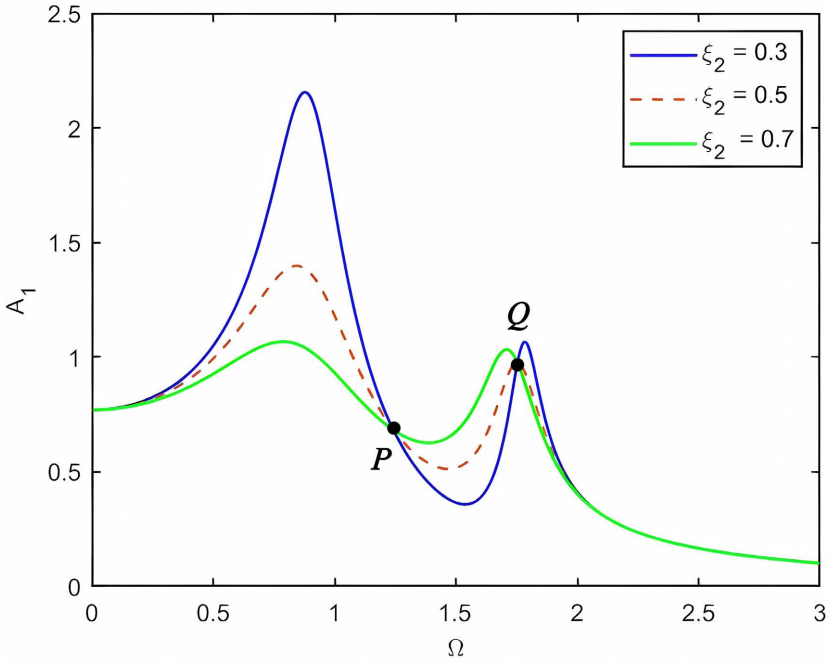

Figure 2. Normalized amplitude-frequency response curves under different damping ratio.

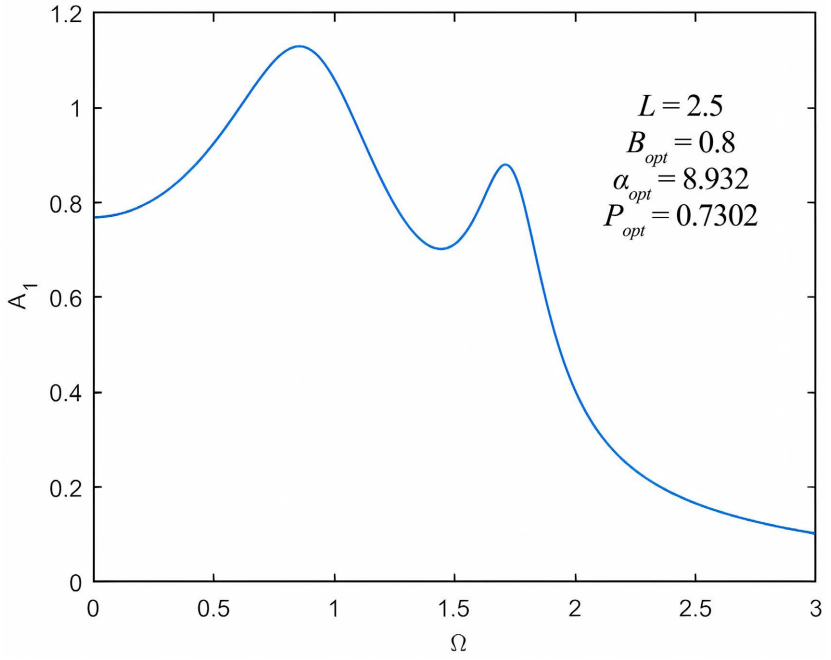

Figure 3. Amplitude-frequency response curve under optimal parameters.

For the grounded stiffness system with an inerter, the reference [25] has calculated the optimal parameters of the system through the fixed-point theory, enabling the two fixed points P and Q to be adjusted to approximately the same height. However, as can be observed from **Figure 3**, for the passive dynamic vibration absorber with the main system having no damping, after optimizing its system parameters using the fixed-point theory, issues such as a narrow vibration reduction frequency band and the amplitude of the main system being highly sensitive to the changes in the excitation frequency near the anti-resonant frequency exist. There is still considerable room for optimizing the amplitude of the main system. Subsequently, time-delay feedback control will be introduced to further reduce the amplitude of the main system and widen the vibration reduction frequency band.

3. Optimization of Anti-Resonance Peak in Time-Delay Feedback Control

3.1. Dynamic Vibration Absorber System with Time-Delay

Under the condition of ensuring the system's stable operation without sacrificing data accuracy, it is necessary to reasonably set the value ranges of the feedback gain coefficient and the time delay. Considering the actual situation of the experimental equipment, the value ranges of g and τ are limited as follows:

$$C_0 = \left\{ (g,\tau) \,|\, 0 \le g \le 2, 0 \le \tau \le 2 \right\} \tag{13}$$

At the same time, define the form of the optimal parameter D_{opt}^i of the system as follows. The parameter D_{opt}^i is the optimal system structural parameter at the i th step, and its value range is $i = 1,2,3,4$. Similar notations that appear subsequently will not be repeated for explanation.

$$D_{\text{opt}}^i = \left\{ \mu, \xi_{1\text{opt}}^i, \xi_{2\text{opt}}, p_{\text{opt}}, \alpha_{\text{opt}}^i, \beta_{\text{opt}}^i, L_{\text{opt}} \right\} \tag{14}$$

Assume that the mass ratio $\mu = m_2/m_1 = 0.1$, and the damping ratio $c_1/c_2 = 10$. According to the relationship in the dimensionless expression (2), the calculation expression for the initial value of the system parameter ξ_{1ori}^1 is 0.2505. By combining with the optimal values of the passive system provided in the reference [25], the specific values of the optimal parameters in the first step are as follows:

$$\begin{aligned} D_{\text{opt}}^1 &= \left\{ \mu, \xi_{1\text{opt}}^1, \xi_{2\text{opt}}, p_{\text{opt}}, \alpha_{\text{opt}}^1, \beta_{\text{opt}}^1, L_{\text{opt}} \right\} \\ &= \left\{ 0.1, 0.2505, 1.0279, 0.7302, 8.923, 0.8, 2.5 \right\} \end{aligned} \tag{15}$$

3.2. Stability Analysis

In the dynamic model of the coupled system established in the previous section, the introduction of the time-delay feedback control system will affect the stability of the system. When solving for the range of the optimal parameters, it is necessary to conduct a stability analysis of the feedback gain coefficient g and the time delay τ, so as to obtain the value ranges of g and τ. First, perform a

Laplace transform on Equation (3), and represent it in the following matrix form in the Laplace domain:

$$\boldsymbol{E}(s)\boldsymbol{X}(s)=\boldsymbol{F}(s) \tag{16}$$

where:

$$\begin{cases} \boldsymbol{X}(s)=\left[\overline{x}_1(s),\overline{x}_2(s)\right]^{\mathrm{T}} \\ \boldsymbol{E}(s)=\begin{vmatrix} s^2+1+\mu L^2p^2+2s\left(\xi_1+L^2\mu p\xi_2\right)+\beta\mu L^2s^2 & \mu Lp\left(p+2\xi_2 s+pge^{-s\tau}\right)+\beta\mu Ls^2 \\ Lp\left(p+2\xi_2 s\right)+\beta Ls^2 & s^2+p^2+\alpha p^2+2p\xi_2 s+\beta s^2+p^2ge^{-s\tau} \end{vmatrix} \\ \boldsymbol{F}(s)=\left[f,0\right]^{\mathrm{T}} \end{cases}$$

Let the characteristic equation of the system be $\left|\boldsymbol{E}(s)\right|=0$, and then the characteristic equation can be obtained as follows:

$$\begin{aligned} CE\left(g,\tau,D_{opt}^{i}\right)=&\ p^2+p^2\alpha+L^2p^4\alpha\mu+s^4\left(1+\beta+L^2\beta\mu\right) \\ &+s^3\left(2\xi_1+2\beta\xi_1+2p\xi_2+2L^2p\mu\xi_2\right) \\ &+s\left(2p^2\xi_1+2p^2\alpha\xi_1+2p\xi_2+2L^2p^3\alpha\mu\xi_2\right) \\ &+s^2\left(1+p^2+p^2\alpha+\beta+L^2p^2\mu+L^2p^2\alpha\beta\mu+4p\xi_1\xi_2\right) \\ &+e^{-s\tau}\left(gp^2+gp^2s^2+2gp^2s\xi_1\right) \end{aligned} \tag{17}$$

Since the established system model contains a time delay term, the expression of the obtained characteristic equation is a transcendental equation with an exponential term. The solutions of the equation are infinite-dimensional, and there will be an infinite number of characteristic roots. To address this issue, the CTCR [26] method is introduced for analysis. The specific calculation steps are as follows:

1) Define Kernel Hyper curves: When the structural parameters of the system are fixed at a certain specific value, the two-dimensional plane of (g,τ) will give rise to an eigenvalue $s=j\Omega_c,\Omega_c\in R^+,0\le\Omega_c\tau\le 2\pi,0\le g\le 2$, with its real part being equal to zero. All the curves composed of points that exist within the two-dimensional plane (g,τ) and satisfy the given conditions are referred to as KH.

2) Define Offspring Hyper curves: The representation of OH can be obtained from Definition 1) through the following non-linear transformation:

$$\left\langle \tau\pm\frac{2\pi}{\Omega_c}i,g\right\rangle,i=0,1,2,3,\cdots. \tag{18}$$

3) Define the variation trend of the characteristic root Root Tendency as:

$$RT=\operatorname{sgn}\left[\operatorname{Re}\left(\left.\frac{\partial s}{\partial\tau}\right|_{s=j\Omega_c}\right)\right] \tag{19}$$

4) Replace the exponential term using Euler's formula:

$$e^{-j\Omega_c\tau}=\cos\left(h_c\right)-j\sin\left(h_c\right),h_c=\Omega_c\tau \tag{20}$$

Among them, the trigonometric functions cos and sin can be replaced by the half-angle formulas when the tangent function tan :

$$\cos\left(h_c\right)=\frac{1-z_1^2}{1+z_1^2},\sin\left(h_c\right)=\frac{2z_1}{1+z_1^2},z_1=\tan\left(\frac{h_c}{2}\right) \tag{21}$$

Continue to use the CTCR method to determine the stability of the system. Substitute the results obtained from Equations (19) and (20) into Equation (17), and the characteristic equation of the system can be rewritten in the form of a polynomial function of Ω_c :

$$q\left(\Omega_c,g,z_1\right)=\sum_{k=0}^{4}c_k\left(g,z_1\right)\left(\Omega_c j\right)^k=0 \tag{22}$$

Among them, c_k is the coefficient expression of Ω_c and is a function of g,z_1. By separating the real and imaginary parts of Equation (22), we can obtain:

$$\begin{cases}\mathrm{Re}\left[q\left(\Omega_c,g,z_1\right)\right]=\sum_{k=0}^{4}Q_k\left(g,z_1\right)\left(\Omega_c\right)^k=0\\ \mathrm{Im}\left[q\left(\Omega_c,g,z_1\right)\right]=\sum_{k=0}^{4}P_k\left(g,z_1\right)\left(\Omega_c\right)^k=0\end{cases} \tag{23}$$

Among them, both P_k and Q_k are coefficient expressions of Ω_c, and they are also functions of g,z_1. The specific results are as follows:

$$\begin{cases}Q_4=\left(1+L^2\beta\mu+\beta+z_1^2+\beta z_1^2+L^2\beta\mu z_1^2\right)\\ Q_3=0\\ Q_2=-1-p^2-gp^2-p^2\alpha-\beta-L^2p^2\mu-z_1^2-L^2p^2\alpha\beta\mu-p^2z_1^2\\ \qquad +gp^2z_1^2-p^2\alpha z_1^2-\beta z_1^2-L^2p^2\mu z_1^2-L^2p^2\alpha\beta\mu z_1^2-4p\xi_1\xi_2-4pz_1^2\xi_1\xi_2\\ Q_1=4gp^2z_1\xi_1\\ Q_0=p^2+gp^2+p^2\alpha+L^2p^4\alpha\mu+p^2z_1^2-gp^2z_1^2+p^2\alpha z_1^2+L^2p^4\alpha\mu z_1^2\\ P_4=0\\ P_3=-2\xi_1-2\beta\xi_1-2z_1^2\xi_1-2\beta z_1^2\xi_1-2p\xi_2-2L^2p\mu\xi_2-2pz_1^2\xi_2-2L^2p\mu z_1^2\xi_2\\ P_2=2gp^2z_1\\ P_1=2p^2\xi_1\left(1+g+\alpha+z_1^2-gz_1^2+\alpha z_1^2\right)+2p\xi_2\left(1+L^2p^2\alpha\mu+z_1^2+L^2p^2\alpha\mu z_1^2\right)\\ P_0=-2gp^2z_1\end{cases} \tag{24}$$

By combining Equation (23), Ω_c can be obtained. Its necessary and sufficient condition needs to be derived through the discriminant and the Dixon resultant. According to the Dixon resultant, assume that:

$$\begin{cases}q_1\left(\Omega_c\right)\equiv\mathrm{Re}\left[q\left(\Omega_c,g,z_1\right)\right]\\ q_2\left(\Omega_c\right)\equiv\mathrm{Im}\left[q\left(\Omega_c,g,z_1\right)\right]\\ \delta\left(\Omega_c,\phi\right)\equiv\frac{1}{\left(\Omega_c,\phi\right)}=\begin{vmatrix}q_1\left(\Omega_c\right) & q_2\left(\Omega_c\right)\\ q_1\left(\phi\right) & q_2\left(\phi\right)\end{vmatrix}\end{cases} \tag{25}$$

Among them, $q_1\left(\phi\right)$ and $q_2\left(\phi\right)$ are obtained by replacing δ with the imaginary variable Ω_c. The expressions of $q_1\left(\phi\right)$ and $q_2\left(\phi\right)$ are as follows:

$$\begin{cases} q_1 = \left(1+L^2\beta\mu+\beta+z_1^2+\beta z_1^2+L^2\beta\mu z_1^2\right)\Omega_c^4+\left(-1-p^2\right. \\ \quad -gp^2-p^2\alpha-\beta-L^2p^2\mu-z_1^2-L^2p^2\alpha\beta\mu-p^2z_1^2+gp^2z_1^2-p^2\alpha z_1^2 \\ \quad \left.-\beta z_1^2-L^2p^2\mu z_1^2-L^2p^2\alpha\beta\mu z_1^2-4p\xi_1\xi_2-4pz_1^2\xi_1\xi_2\right)\Omega_c^2+L^2p^4\alpha\mu z_1^2 \\ \quad +4gp^2z_1\xi_1\Omega_c+p^2+gp^2+p^2\alpha+L^2p^4\alpha\mu+p^2z_1^2-gp^2z_1^2+p^2\alpha z_1^2 \\ q_2 = \left(-2\xi_1-2\beta\xi_1-2z_1^2\xi_1-2\beta z_1^2\xi_1-2p\xi_2-2L^2p\mu\xi_2-2pz_1^2\xi_2\right. \\ \quad \left.-2L^2p\mu z_1^2\xi_2\right)\Omega_c^3+2gp^2z_1\Omega_c^2+\left[2p^2\xi_1\left(1+g+\alpha+z_1^2-gz_1^2+\alpha z_1^2\right)\right. \\ \quad \left.+2p\xi_2\left(1+L^2p^2\alpha\mu+z_1^2+L^2p^2\alpha\mu z_1^2\right)\right]\Omega_c-2gp^2z_1 \end{cases} \tag{26}$$

Through observation, it can be found that Equation (25) is a polynomial of $deg-1$ that is symmetric about σ and Ω_c, and it can also be understood as a Dixon polynomial about $q_1(\Omega_c)$ and $q_2(\Omega_c)$. Due to its symmetric property, changing the positions of the elements within the expression will not change its result, that is, $\delta(\Omega_c,\phi)=\delta(\phi,\Omega_c)$. The above-mentioned $deg-1$ represents the highest order of Ω_c in $q_1(\Omega_c)$ and $q_2(\Omega_c)$. Among them, $deg=\max\left(deg\left(q_1(\Omega_c)\right),deg\left(q_2(\Omega_c)\right)\right)$, $deg\left(q_1(\Omega_c)\right)$ and $deg\left(q_2(\Omega_c)\right)$ also represent the highest order terms about Ω_c. Any common zero point of $q_1(\Omega_c)$ and $q_2(\Omega_c)$ is also a zero point of $\delta(\Omega_c,\phi)$ corresponding to ϕ. Therefore, under the condition of the common zero point, the coefficient of the coefficient $\delta(\Omega_c,\phi)$ in ϕ^i is zero, which can be expressed in matrix form as follows:

$$\boldsymbol{D}(g,z_1)=\begin{pmatrix}1\\ \Omega_c\\ \vdots\\ \Omega_c^{deg-1}\end{pmatrix}=\begin{pmatrix}0\\0\\ \vdots\\0\end{pmatrix} \tag{27}$$

Among them, $i=0,1,2,3,\cdots,deg-1$. The coefficient matrix $\boldsymbol{D}(g,z_1)\in R^d$ is called the Dixon matrix, and $d=deg\times deg$.

$$\boldsymbol{D}(g,z_1)=\begin{pmatrix}D_1 & D_2 & D_3 & D_4\\ D_5 & D_6 & D_7 & D_8\\ D_9 & D_{10} & D_{11} & D_{12}\\ D_{13} & D_{14} & D_{15} & D_{16}\end{pmatrix} \tag{28}$$

When the matrix $\boldsymbol{D}(g,z_1)$ is a singular matrix, a non-trivial solution of Equation (26) can be obtained, that is: $deg=\left[\boldsymbol{D}(g,z_1)\right]=0$. When g is within a specific value range, Equation (28) will transform into a 16th-degree polynomial about z_1:

$$R_z=\sum_{l=0}^{16}R_l(g)z_1^l=0 \tag{29}$$

Among them, $l=0,1,2,\cdots,16$. The specific expression of the coefficient $R_l(g)$ is quite complex and will not be presented in detail. To obtain the stable interval ranges of the feedback gain coefficient and the time delay amount, the above algebraic expressions will be numerically solved according to the following steps:

1) Given the initial value of the parameter g, find the roots of the equation

$deg = \left[\boldsymbol{D}(g, z_1)\right] = 0$, and substitute the real roots into Equation (21) to obtain the value of h_c.

2) Substitute h_c into Equation (20) to obtain the value of $e^{-j\Omega_c\tau}$. Then substitute this value into the characteristic Equation (17), and all the characteristic roots can be obtained.

3) Among the obtained characteristic roots, filter out the pure imaginary roots and mark them as Ω_c. Substitute the obtained Ω_c and h_c into the characteristic Equation (17) to obtain the time delay amount $\tau_i, i = 1, 2, 3, 4, \cdots$

4) Change the value of the feedback gain coefficient g to make it linearly increase within a certain range until the value of g reaches the set value, and repeat the above steps to obtain $C_1 = \left\{(g, \tau) \,|\, \mathrm{Re}\left(CE(D, g, \tau) < 0\right)\right\} \cap C_0$. The parameter ranges are as follows:

$$D = \{\mu, \xi_1, \xi_2, p, \alpha, \beta, L\} = \{0.1, 0.1 \sim 0.9, 0 \sim 2, 0.7302, -2 \sim 9, 0.4923 \sim 2.5846, 2.5\};$$

3.3. Optimization Criterion for Anti-Resonance Points

When optimizing system parameters, the selection of optimization algorithm is particularly important. In order to achieve accurate vibration suppression of key frequencies and broaden the frequency band of vibration reduction, the anti-formant optimization criterion can solve the vibration problem of specific frequencies more directly than its optimization method, and achieve the purpose of wideband vibration reduction through reasonable parameter design.

Next, regarding the system's system of differential equations of motion (3), the amplitude optimization problem of the anti-resonance points is studied by adopting time-delay feedback active control. The time delay is used to control the amplitude of the anti-resonance points and the position of the anti-resonance frequencies, and a criterion for minimizing the amplitude of the anti-resonance points is designed. To achieve this goal, it is first necessary to obtain the frequencies and amplitudes of the anti-resonance points, and then use the minimum value of the function to derive the conditions for the minimum amplitude of the main system as follows:

$$\begin{aligned} &\frac{\mathrm{d}A_1}{\mathrm{d}\Omega} = 0 \\ &\frac{\mathrm{d}^2 A_1}{\mathrm{d}\Omega^2} > 0 \end{aligned} \tag{30}$$

Among them, $\mathrm{d}A_1/\mathrm{d}\Omega$ and $\mathrm{d}^2A_1/\mathrm{d}\Omega^2$ are obtained according to the amplitude magnification factor expression (7). For a two-degree-of-freedom linear system, the conditions for finding the anti-resonance points are the same as the conditions for the minimum value of the amplitude of the main system. According to the above conditions for the minimum value of the system amplitude, the frequencies of the anti-resonance points can be obtained. Substituting these frequencies into the expression (7) of the amplitude magnification factor can yield the amplitudes of the anti-resonance points. For the given system structure parameter $D = \{\mu, \xi_1, \xi_2, p, \alpha, \beta, L\}$, subsequently, by changing the feedback gain coefficient

and the time-delay amount, the amplitudes of the anti-resonance points can be adjusted to make them within a sufficiently small range, which is defined as: $\min\left\|A_1\left(D,\Omega_c,g,\tau\right)\right\|<10^{-1}$. According to the above, the optimization criterion for satisfying the minimum of the anti-resonance points can be obtained as:

$$\begin{aligned}&\left.\frac{\mathrm{d}A_1}{\mathrm{d}\Omega}\right|_{\Omega=\Omega_{anti}}=0\\&\left.\frac{\mathrm{d}^2A_1}{\mathrm{d}\Omega^2}\right|_{\Omega=\Omega_{anti}}>0\\&\min\left\|A_1\left(D,\Omega_{anti},g,\tau\right)\right\|<10^{-1}\end{aligned}\tag{31}$$

Among them, Ω_{anti} represents the anti-resonance frequency, and $A_1\left(D,\Omega_c,g,\tau\right)$ is the amplitude of the anti-resonance peak of the system. It is assumed that C_2 is not only the interval of g and τ that enables the system to operate stably, but also the stable operating interval of g and τ under the condition of satisfying the minimum criterion of the anti-resonance points of the system. Its specific form is:

$$C_2=\left\{\left(g,\tau\right)\middle|\min\left\|A_1\left(D,\Omega_{anti},g,\tau\right)\right\|<10^{-1}\right\}\cap C_1\tag{32}$$

In order to study the vibration reduction effect of the time-delay feedback active control on the vibration system at the anti-resonance points, taking the optimal structural parameter D_{opt}^1 obtained in the passive system in reference [25] as an example, the anti-resonance frequency $\Omega_a\in\left(0,2\right)$ is restricted, and by changing the time-delay amount and the feedback gain coefficient, the amplitude A_1 of the main system at the anti-resonance frequency can be obtained. The amplitude-frequency response curve of the time-delay feedback control is shown in **Figure 4**.

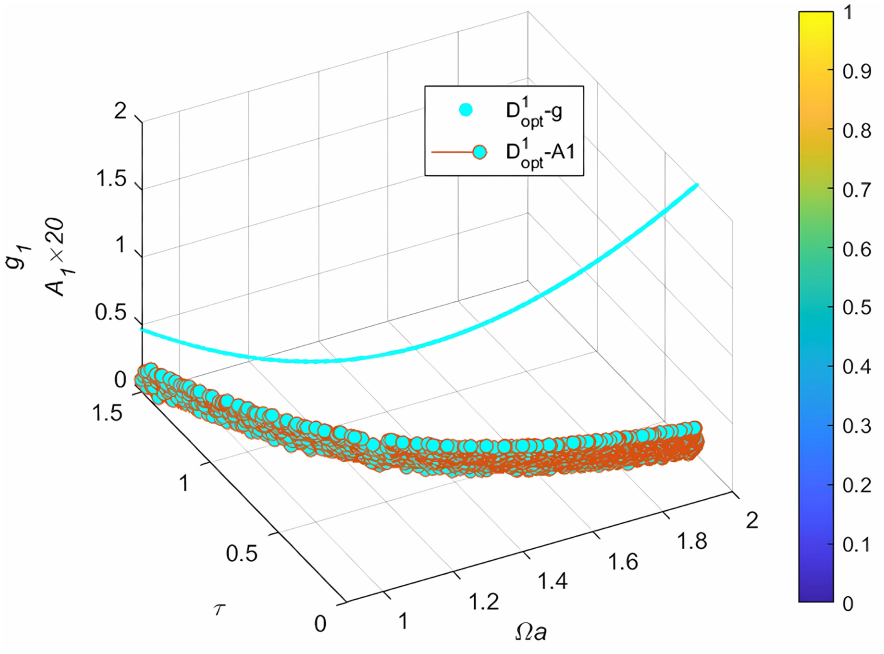

Figure 4. The amplitude-frequency response curve of the time-delay active control.

Within the optimization criterion that the anti-resonance amplitude is less than 0.01, there is an adjustable interval of the feedback gain coefficient g and the time-delay amount τ within the range of $\Omega_a \in (0,2)$. However, it can be found from the figure that the time-delay feedback active control is mainly concentrated in the high-frequency region, and when the anti-resonance frequency is small, the time-delay feedback control will fail. Therefore, it is necessary to optimize the design of the system structural parameters D in combination with the time-delay feedback control, so that it can achieve the best optimization effect while having a wide vibration reduction frequency band and frequency band symmetry.

According to the above optimization requirements, the initial values for the optimization of the vibration system are given as follows:

$$D_0 = \left\{\mu, \xi_1, \xi_2, p, \alpha^0, \beta, L\right\} = \left\{0.1, 0.2505, 1.0279, 0.7302, 0, 0.8, 2.5\right\} \tag{33}$$

Then, within the range of structural parameter optimization, the difference between the initial parameter D_0 and the final parameter D is divided into N equal parts, and incremental searches are carried out step by step to obtain the optimal parameters. In order to ensure the accuracy of the data and at the same time shorten the search time, $N = 100$ is taken, and the calculation step size is $\Delta_D = (D_0 - D)/N$. The structural parameter of the $(h+1)^{th}$ step is set as $D_{h+1} = D_h + \Delta_D$, where D_h is the structural parameter of the h^{th} step and $h = 0, 1, 2, \cdots, N$.

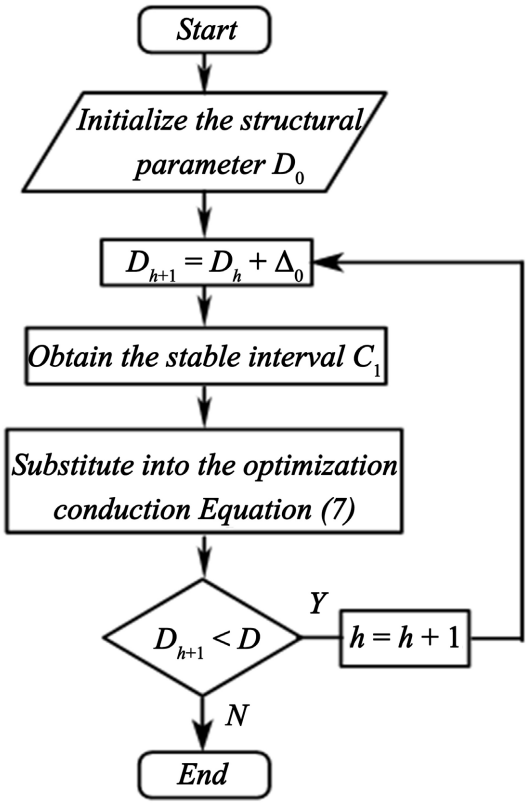

Figure 5. Flowchart for the calculation of anti-resonance points.

Finally, by substituting the structural parameter D_{h+1} into Expressions (31) and (32), the feedback gain coefficient g and the time delay τ corresponding to the condition that satisfies the minimum amplitude criterion of the anti-resonance points can be obtained. The specific process is shown in Figure 5.

3.4. Optimization of the Grounding Negative Stiffness α

The ground negative stiffness absorber uses a special structure to generate negative stiffness force, which presents a nonlinear relationship between force and displacement, and can more effectively offset or reduce the exciting force under specific vibration conditions, and rapidly suppress vibration to achieve better vibration reduction effect. Its implementation principle is shown in Figure 6.

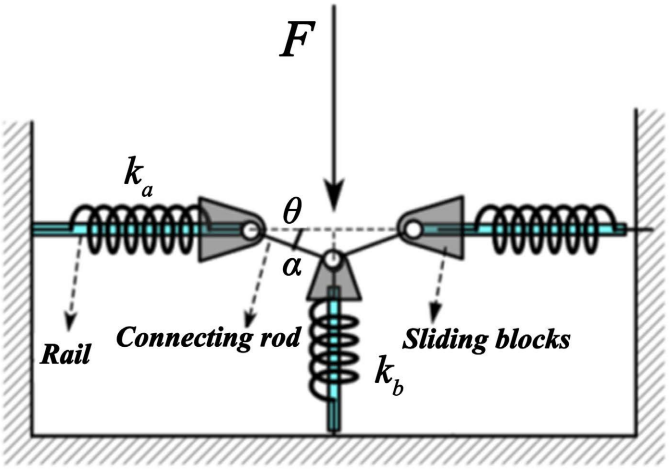

Figure 6. Schematic diagram of the negative stiffness device.

The two springs in the horizontal plane are preloaded springs, one end of the spring is fixed on the support, and the other end is connected with the linear bearing slider. The cylindrical guide rail plays a role in fixing and limiting the slider and the spring, and the slider can slide freely along the cylindrical guide rail. Among them, the stiffness of the two horizontal springs is k_a, the stiffness of the vertical spring is k_b, the angle between the horizontal spring and the connecting rod is θ, the original length of the horizontal spring is L_0, the spring compression of the horizontal spring in the equilibrium position is h, and the length of the two connecting rods is a. When the connecting rod is in the horizontal position, the vertical spring does not deform.

When the displacement in the vertical direction is x, the following expression is obtained:

$$F = k_b x - 2\frac{x}{\sqrt{a^2 - x^2}}\left(h - a + \sqrt{a^2 - x^2}\right)k_a \tag{34}$$

After derivation of displacement by formula (34), and then dimensionless quantization simplification, the relationship between dimensionless stiffness and dimensionless displacement can be obtained as follows:

$$\overline{K_3} = 1 - 2d\left(\frac{d_1 - d_2 + \sqrt{d_2^2 - \overline{x^2}} + \overline{x^2}(d_1 - d_2)}{d_2^2 - \overline{x^2}}\right) \tag{35}$$

In formula (35), the force-displacement relationship of the horizontal negative stiffness device is completely derived. According to Taylor expansion, it can be seen that under the condition of small displacement, the higher-order nonlinear term can be ignored, and the device has good robustness.

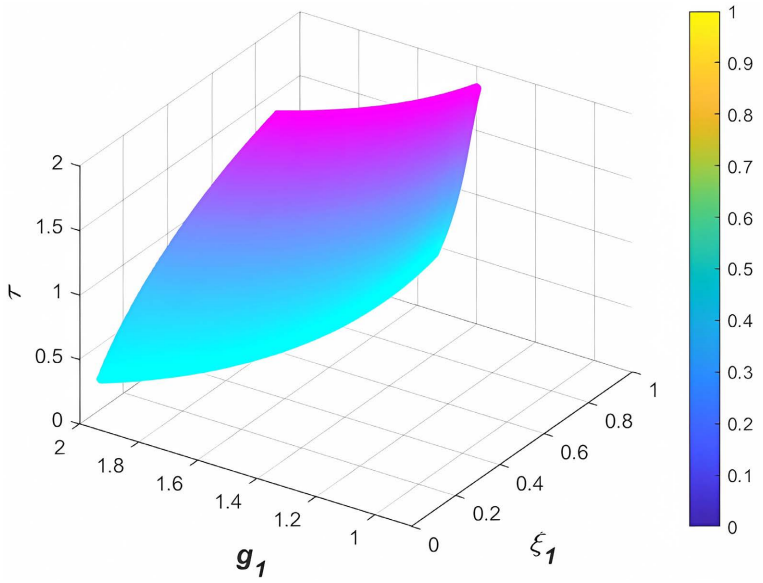

(a)

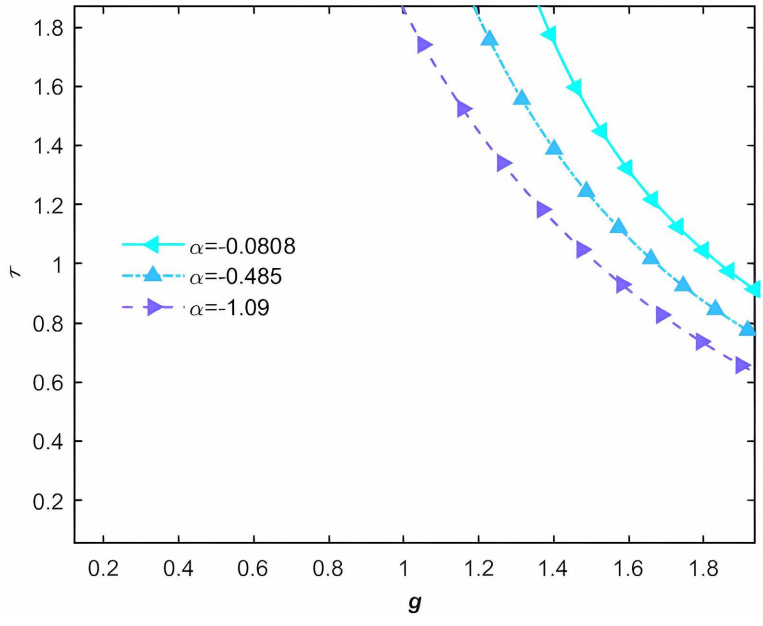

(b)

Figure 7. The stable intervals of the time-delay amount and the feedback gain coefficient under different values of α. (a) Three-dimensional diagram of the stable interval of g and τ (b) Two-dimensional cross-sectional diagram of the stable interval of g and τ.

According to the above calculation process of the anti-resonance points, the optimization design of the system parameter α is carried out first. The values of other system parameters are all those in D_{opt}^1. A value interval is given for the stiffness coefficient α so that the optimal value of the stiffness coefficient α in D_{opt}^1 lies within this interval. The specific structural parameter D_{opt}^1 is as follows:

$$D = \{\mu, \xi_1, \xi_2, p, \alpha, \beta, L\} = \{0.1, 0.2505, 1.0279, 0.7302, -2 \sim 9, 0.8, 2.5\} \quad (36)$$

After determining the values of the above structural parameters, the stability region diagram of the stiffness coefficient, the feedback gain coefficient and the time delay is drawn as follows:

From Figure 7, it can be found that when α is within the range of $(-2,0)$, there exists an adjustable interval for the feedback gain coefficient g and the time delay τ. Moreover, as the stiffness coefficient α continuously increases, the adjustable interval for the feedback gain coefficient and the time-delay amount also keeps expanding. When $\alpha \in (0,9)$, since a stable g, τ interval has not been found, the stability diagram of this region is not presented in the figure.

Figure 8(a) and Figure 8(b) represent the relationship diagrams between the anti-resonance frequency range of g and τ, the amplitude A_1 of the anti-resonance point under different stiffness coefficients α. It can be seen from Figure 8(b) that when $\alpha \in [-1.616, -0.8081]$, as the stiffness coefficient α continuously increases, the adjustable width of the anti-resonance frequency gradually increases; when , as the stiffness coefficient α continuously increases, the adjustable width of the anti-resonance frequency gradually decreases. From the perspective of controlling the symmetry of the anti-resonance frequency band, there exists an optimal stiffness coefficient α in Figure 8(c). While ensuring that both g and τ are within the stable range, the frequency band width of its anti-resonance point also maintains a certain symmetry with the main resonance point.

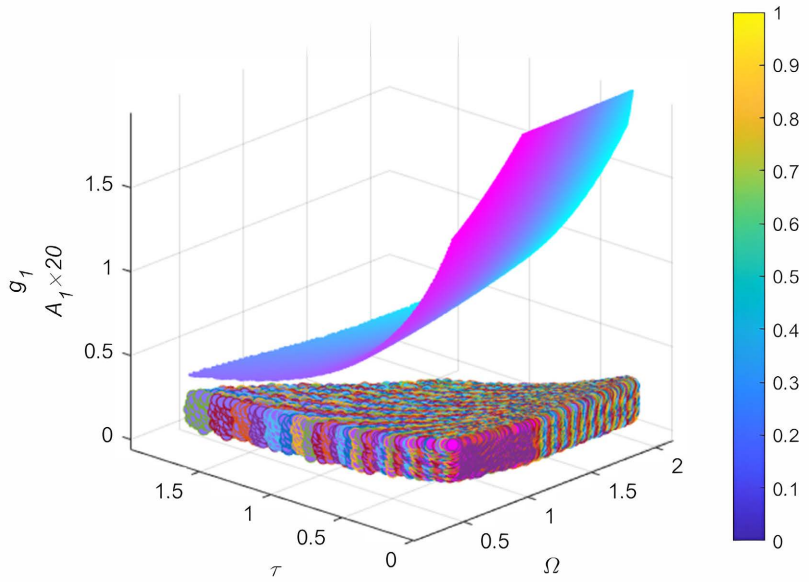

(a)

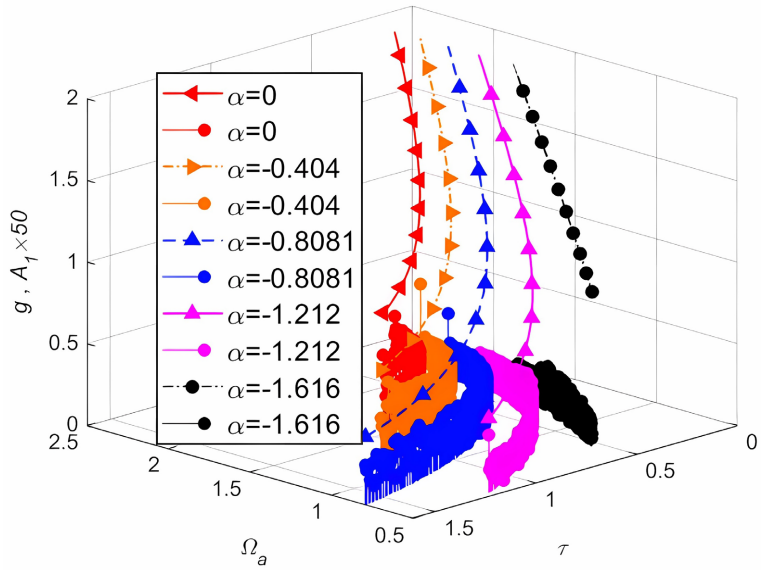

(b)

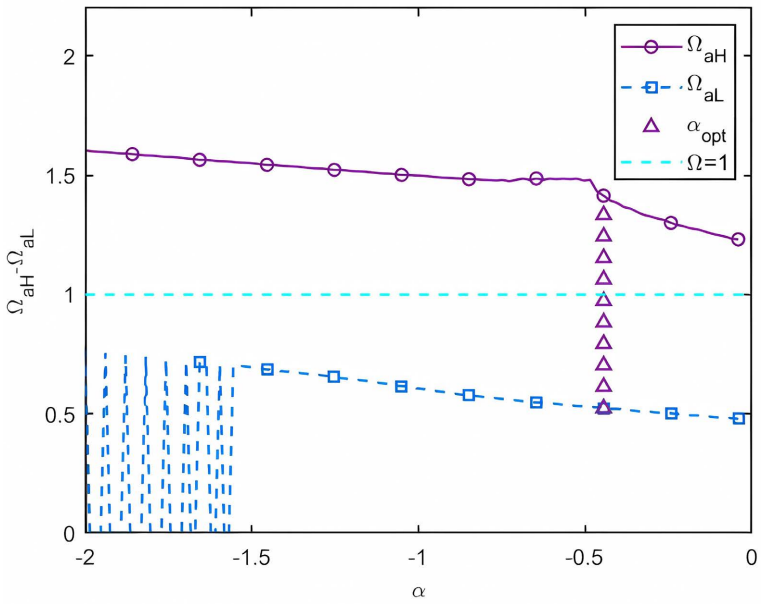

(c)

Figure 8. The anti-resonance frequency adjustment range and the minimum anti-resonance frequency amplitude of the g and τ at different α values. (a) Three-dimensional diagram of the relationship between the anti-resonance frequency range and the amplitude (b) Cross-section of the three-dimensional diagram (c) Two-dimensional diagram of the optimal α.

Record the stiffness coefficient $\alpha_{\text{opt}}^2 = -1.4444$ marked by the purple triangle in **Figure 8(c)** as the optimal value. The specific range of the adjustable anti-resonance frequency band corresponding to this point is $(\Omega_{aL}, \Omega_{aH}) = (0.5606, 1.4434)$. Take the value of the above optimal stiffness coefficient α as the initial value for the second-step optimization. At this time, the optimal structural parameters of the system are as follows:

$$D_{\text{opt}}^2 = \left\{\mu, \xi_1, \xi_2, p, \alpha^2, \beta, L\right\} = \left\{0.1, 0.2505, 1.0279, 0.7302, -1.4444, 0.8, 2.5\right\} \quad (37)$$

Under these structural parameters, the requirement for the symmetry of the adjustable anti-resonance point frequency band still has a large gap compared with the expected value, and it is necessary to further optimize other parameters.

3.5. Optimization of the Main System Damping ξ_1

Next, carry out the optimization design of the system parameter ξ_1. Similarly,

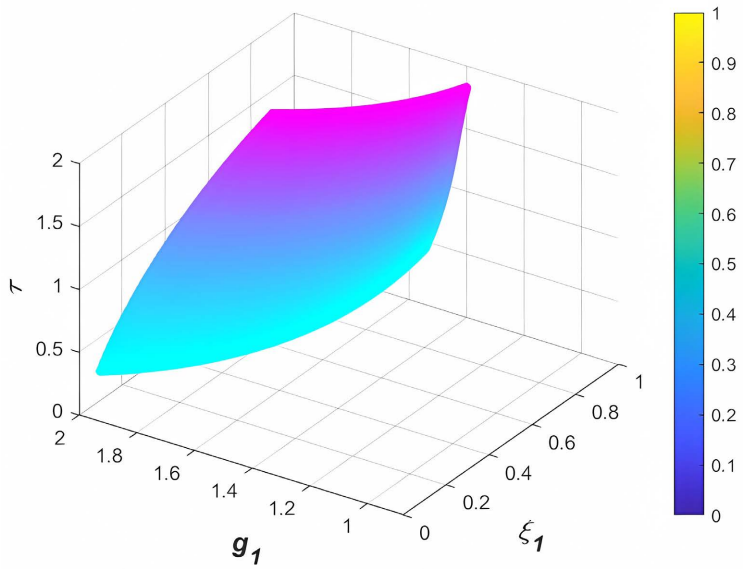

(a)

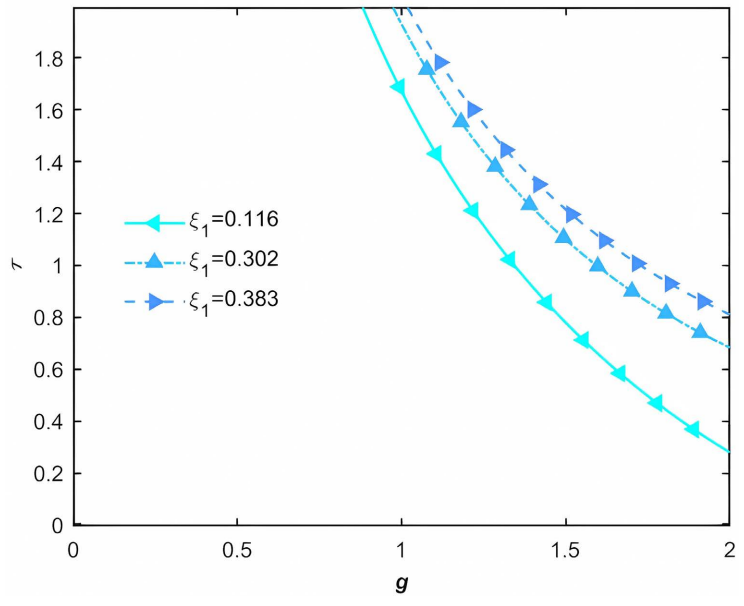

(b)

Figure 9. The stable intervals of the time-delay amount and the feedback gain coefficient under different values of ξ_1. (a) Three-dimensional diagram of the stable interval of g and τ (b) Two-dimensional cross-sectional diagram of the stable interval of g and τ.

follow the above calculation process of the anti-resonance points. The values of other system parameters are all those in D_{opt}^2. Give a value interval for the stiffness coefficient ξ_1 so that the optimal value of the damping coefficient ξ_1 in D_{opt}^2 is within this range. The specific structural parameter D_{opt}^2 is as follows:

$$D=\{\mu,\xi_1,\xi_2,p,\alpha,\beta,L\}=\{0.1,0.1\sim 0.9,1.0279,0.7302,-1.4444,0.8,2.5\} \quad (38)$$

After determining the values of the above structural parameters, the stability region diagram of the main system damping, the feedback gain coefficient and the time delay is drawn as shown in **Figure 9**.

It can be found from **Figure 9** that when ξ_1 is within the range of $(0.1,0.9)$, there exists an adjustable interval for the feedback gain coefficient g and the time delay amount τ. Moreover, as the main system damping ξ_1 continuously increases, the adjustable interval for the feedback gain coefficient and the time delay amount also keeps expanding.

Figure 10(a) represents the relationship diagram between the anti-resonance frequency range of the time-delay quantity g and the feedback gain coefficient τ and the amplitude A_1 of the anti-resonance point under the main system damping ξ_1. It can be seen from **Figure 10(b)** that there exists an optimal main system damping ξ_1. While ensuring that both g and τ are within the stable range, the frequency band width of its anti-resonance point also maintains good symmetry with the main resonance point.

Record the main system damping $\xi_{1\text{opt}}=0.4797$ marked by the blue five-pointed star in **Figure 10(b)** as the optimal value. The specific range of the adjustable anti-resonance frequency band corresponding to this point is $(\Omega_{aL},\Omega_{aH})=(0.4445,1.6196)$. Take the value of the above optimal main system damping ξ_1 as the initial value for the third-step optimization. At this time, the optimal structural parameters of the system are as follows:

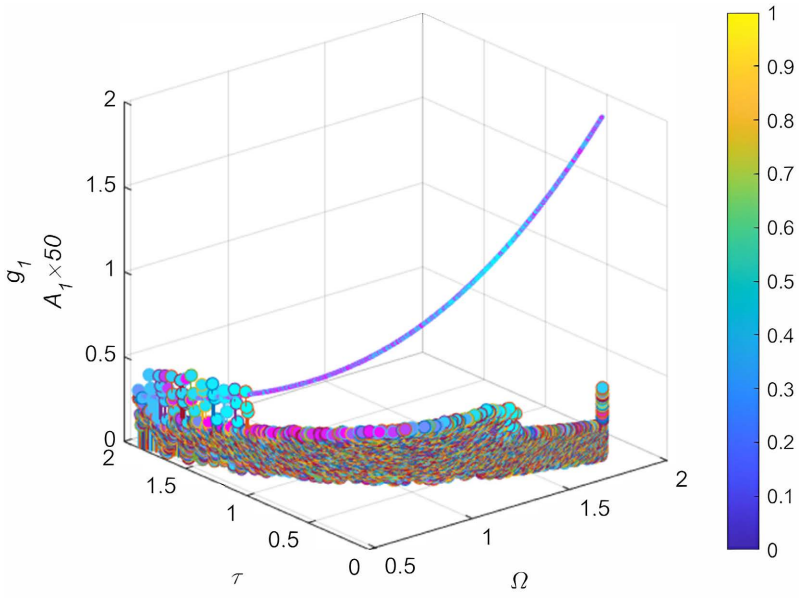

(a)

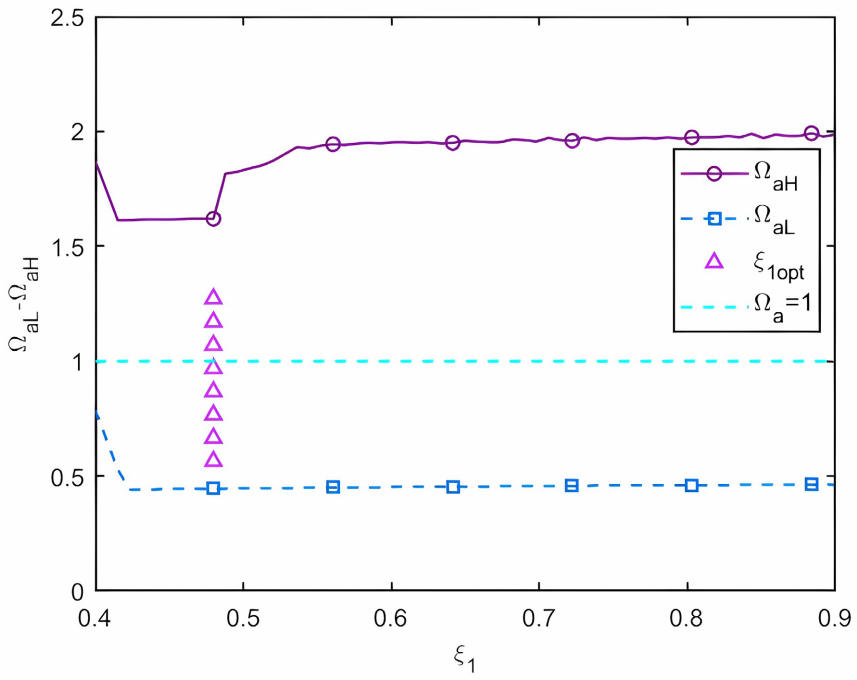

(b)

Figure 10. The anti-resonance frequency adjustment range and the minimum anti-resonance frequency amplitude of the g and τ at different ξ_1 values. (a) Three-dimensional diagram of the relationship between the anti-resonance frequency range and the amplitude (b) Two-dimensional diagram of the optimal ξ_1.

$$D_{\text{opt}}^3 = \left\{\mu, \xi_1^2, \xi_2, p, \alpha^2, \beta, L\right\} = \left\{0.1, 0.4797, 1.0279, 0.7302, -1.4444, 0.8, 2.5\right\} \quad (39)$$

3.6. Optimization of the Main System Damping β

Finally, optimize the inerter ratio. Within the optimal working range of the inerter, select the inerter ratio β that simultaneously meets the best adjustable intervals of g and τ for optimization design. The values of other system parameters are all those in D_{opt}^3. Give a value interval for the inerter ratio β so that the optimal value of the inerter ratio β in D_{opt}^1 is within this range. The specific structural parameter D is shown in Equation (40).

$$D = \left\{\mu, \xi_1, \xi_2, p, \alpha, \beta, L\right\} = \left\{0.1, 0.4797, 1.0279, 0.7302, -1.4444, 0.4 \sim 2.5, 2.5\right\} \quad (40)$$

After determining the values of the above structural parameters according to the cyclic process, the stability region diagram of the main system damping, the feedback gain coefficient and the time delay is drawn as follows:

It can be found from **Figure 11** that when β is within the range of $(0, 2.48)$, there exists an adjustable interval for g and τ. Moreover, as the inerter ratio β continuously decreases, the adjustable interval for the feedback gain coefficient g and the time-delay quantity τ keeps expanding.

Figure 12(a) shows the relationship diagram between the anti-resonance frequency range of g and τ. and the amplitude A_1 of the anti-resonance point

under the inerter ratio β. As can be seen from Figure 12(b), there exists an optimal inerter ratio β. While ensuring that both g and τ. are within the stable range, the frequency-band width of its anti-resonance point maintains good symmetry with the main resonance point.

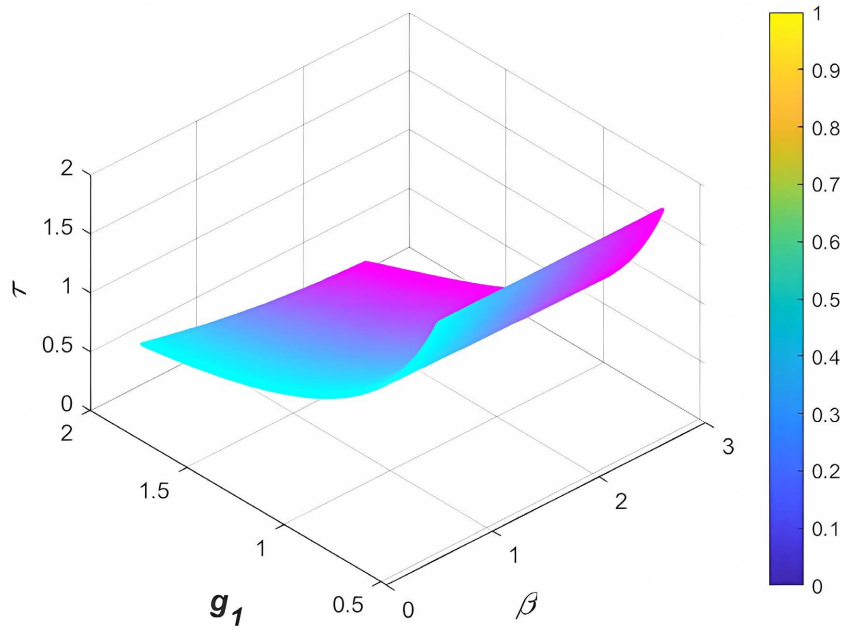

(a)

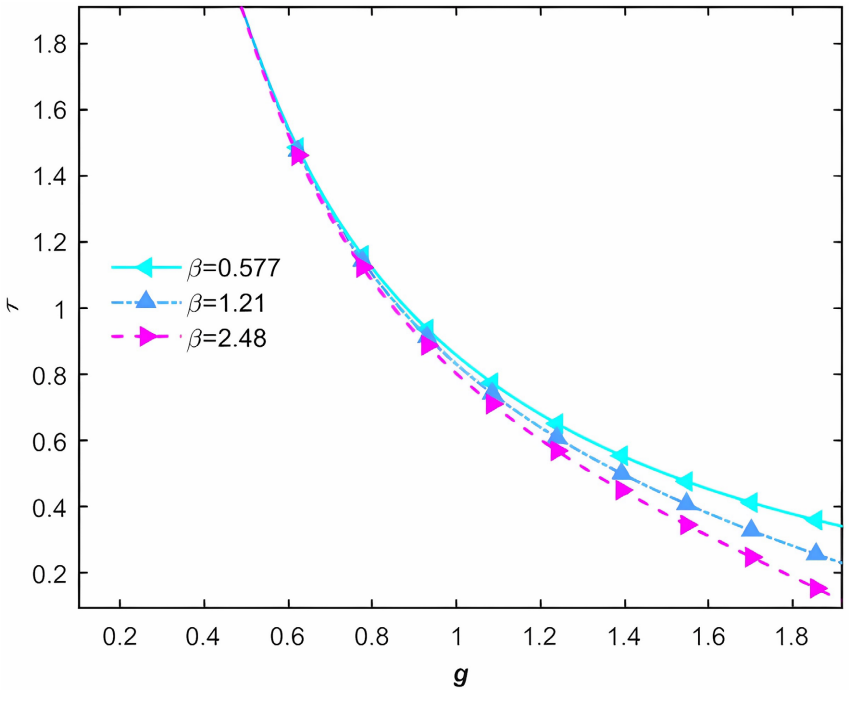

(b)

Figure 11. The stable intervals of the time-delay amount and the feedback gain coefficient under different values of β. (a) Three-dimensional diagram of the stable interval of g and τ (b) Two-dimensional cross-sectional diagram of the stable interval of g and τ.

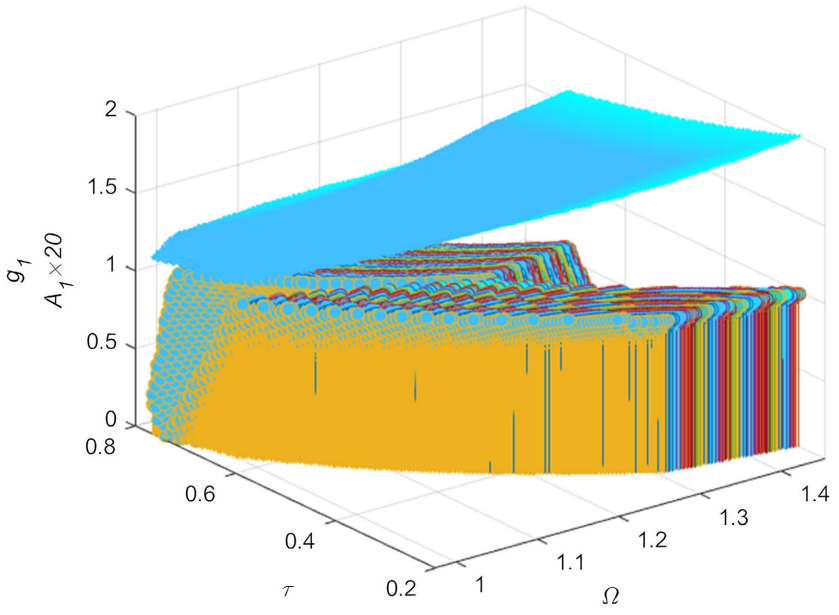

(a)

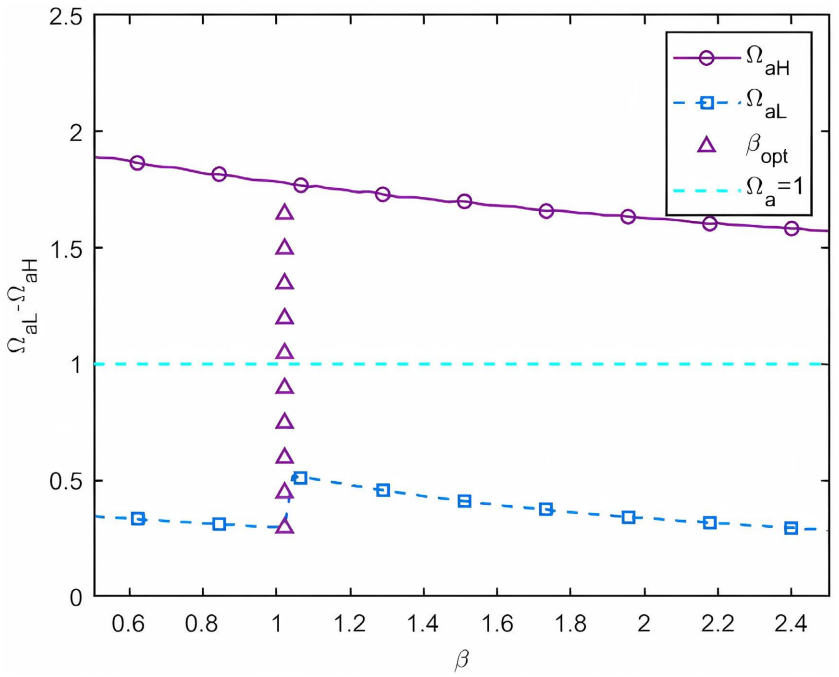

(b)

Figure 12. The anti-resonance frequency adjustment range and the minimum anti-resonance frequency amplitude of the g and τ at different β values. (a) Three-dimensional diagram of the relationship between the anti-resonance frequency range and the amplitude (b) Two-dimensional diagram of the optimal β.

Record the inerter ratio $\beta=1.0222$ marked by the triangle in **Figure 12(b)** as the optimal value. The specific range of the adjustable anti-resonance frequency band corresponding to this point is $(\Omega_{aL},\Omega_{aH})=(0.2965,1.7809)$. Take the value of the above optimal inerter ratio β as the initial value for the fourth-step

optimization. At this time, the optimal structural parameters of the system are as follows:

$$D_{opt}^{4}=\left\{\mu,\xi_1^2,\xi_2,p,\alpha^2,\beta^2,L\right\}=\left\{0.1,0.7390,1.0279,0.7302,-1.444,1.0222,2.5\right\} \quad (41)$$

4. Verification and Analysis

In the third subsection, the optimal structural parameters of the time-delay feedback control system were obtained by using the anti-resonance point optimization criterion, as shown in Table 1. D_1 represents the optimal parameters when there is no active control of the main system damping and time-delay feedback. $D_2 \sim D_4$ represents the results of gradual optimization after the introduction of active control of the main system damping and time-delay feedback. Among them, D_4 represents the optimal parameters after the optimization is completed.

Table 1. Optimal structural parameters.

Structural parameters	D_1	D_2	D_3	D_4
μ	0.100	0.100	0.100	0.100
ξ_1	0.2505	0.2505	0.4797	0.4797
ξ_2	1.0279	1.0279	1.0279	1.0279
p	0.7302	0.7302	0.7302	0.7302
β	0.800	0.800	0.800	1.0222
α	8.923	−1.4444	−1.4444	−1.4444
L	2.5	2.5	2.5	2.5

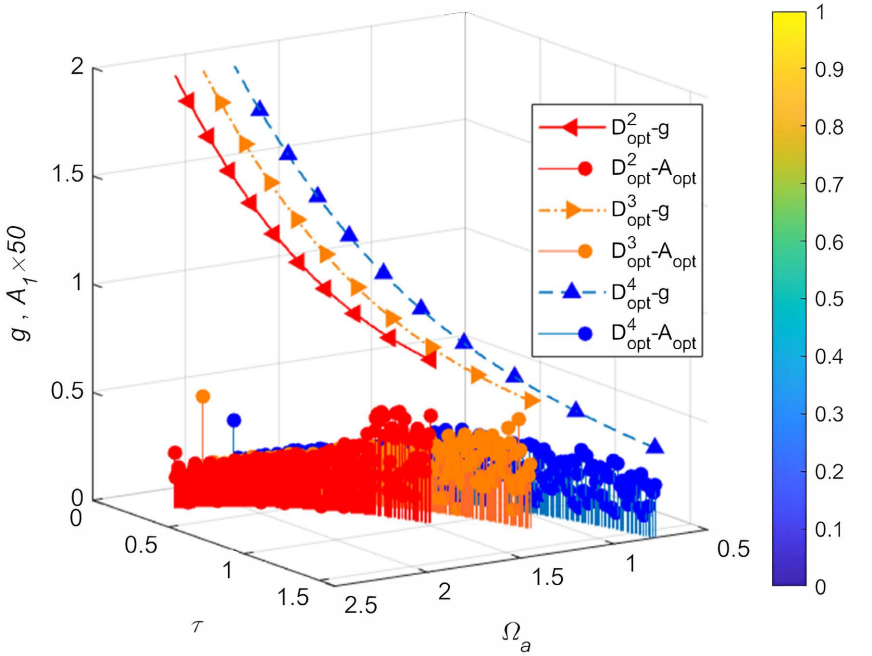

Figure 13. The anti-resonance frequency range of g and τ, and the minimum amplitude at the corresponding frequencies.

In this chapter, by applying the cyclic flowchart shown in Figure 5, the anti-resonance frequency range and the minimum amplitude diagram at the corresponding frequencies for the optimization results of the structural parameters at each step in $D_2 \sim D_4$ are obtained. The comparison results are shown in Figure 13.

In order to verify the effectiveness of the anti-resonance point optimization method, this subsection will verify the above optimization results. The optimal structural parameters D_4 will be selected and substituted into the characteristic equation of the system, and stability verification, frequency domain verification and time domain verification will be carried out respectively.

4.1. Stability Verification

Now that the optimal structural parameters D_4 of the system have been obtained, the CTCR method [26] is continuously used to conduct stability verification on the parameters D_4. Replace the structural parameters D in equation C_1 in Subsection 3.2 with the optimal system parameters D_4 to obtain C_3 under the optimal parameter range, that is: ADSDA; Similarly, replace the structural parameters D in equation C_2 in Subsection 3.3 with the optimal system parameters D_4, and replace C_1 with C_3 to obtain the stable interval C_4 of the feedback gain coefficient and the time delay quantity that satisfy the criterion of the minimum amplitude of the anti-resonance point and are stable,

$$C_4 = \left\{(g,\tau) \mid \min \left\| A_1\left(D_4, \Omega_{anti}, g, \tau\right)\right\| < 10^{-2}\right\} \cap C_3;$$

The range of its stable interval is shown in Figure 14. Below the solid blue square line in the figure represents the stable range of C_3, and below the red dotted line represents the stable range of C_4. Select five points of T_1, T_2, T_3, T_4, T_5 at the same interval on C_4. Only T_1, T_3 and T_5 are marked in Figure 14(a), and their coordinates are $(1.541, 0.873)$, $(1.749, 0.703)$ and $(1.749, 0.703)$ respectively.

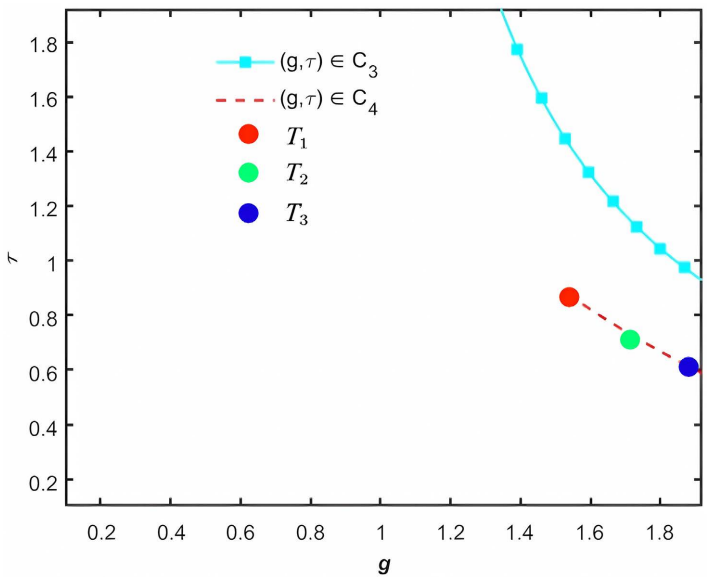

(a)

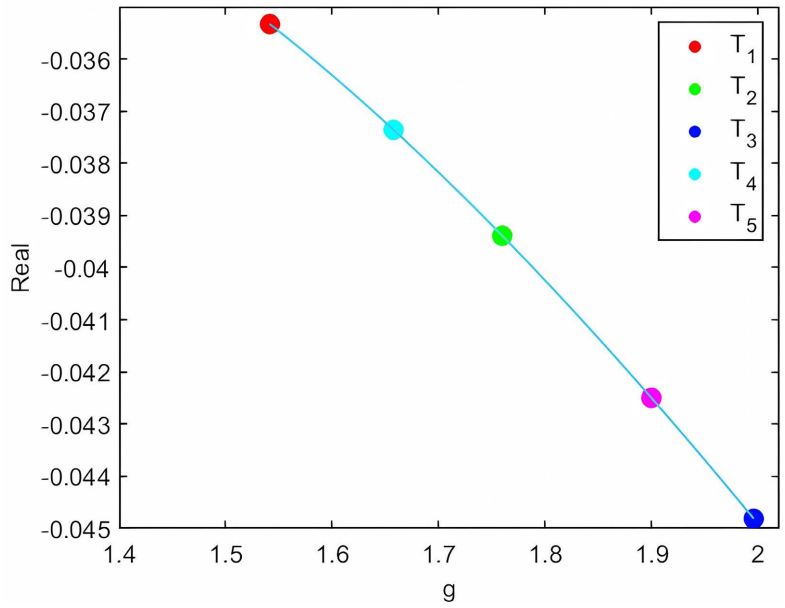

(b)

Figure 14. The stable interval of g and τ under the system parameters D_4. (a) CTCR method (b) Numerical method.

In order to verify that the gain coefficient and time delay corresponding to the points on the C_4 curve can make the system stable, first, substitute the complex number $s=a+ib$ into the characteristic Equation (17) and expand all polynomials; then use Euler's formula $e^{-s\tau}=e^{-a\tau}\left[\cos(b\tau)-i\sin(b\tau)\right]$ to deal with the exponential terms; finally, organize the characteristic equation into the real part $\mathrm{Re}(CE)$ and the imaginary part $\mathrm{Im}(CE)$. Substitute the values of g and τ corresponding to the above five measurement points into the expressions of the real part and the imaginary part, and the structural parameter values are still the optimized structural parameters D_4 in the fourth step. By solving the simultaneous equations of $\mathrm{Re}(CE)=0$ and $\mathrm{Im}(CE)=0$ numerically, the values of a and b can be obtained.

According to the above steps, the characteristic root with the maximum real part of the characteristic Equation (17) is obtained, and the results are shown in Figure 14(b). As can be seen from Figure 14(b), the real parts of the characteristic roots of the five measuring points are all less than 0. This indicates that g and τ on the C_4 curve can make the system stable. Subsequently, the anti-resonance amplitude verification will be carried out by taking the three measuring points marked in Figure 14(a) as examples.

4.2. Frequency Domain and Time Domain Verification

According to Figure 14(a), the values of the corresponding gain coefficient and time delay can be determined. By substituting the coordinates of these three measuring points into Figure 13, the anti-resonance point frequencies Ω_a corresponding to these three points can be determined as: $\Omega_{a1}=0.5135$, $\Omega_{a3}=0.9069$,

$\Omega_{a5} = 1.2762$.

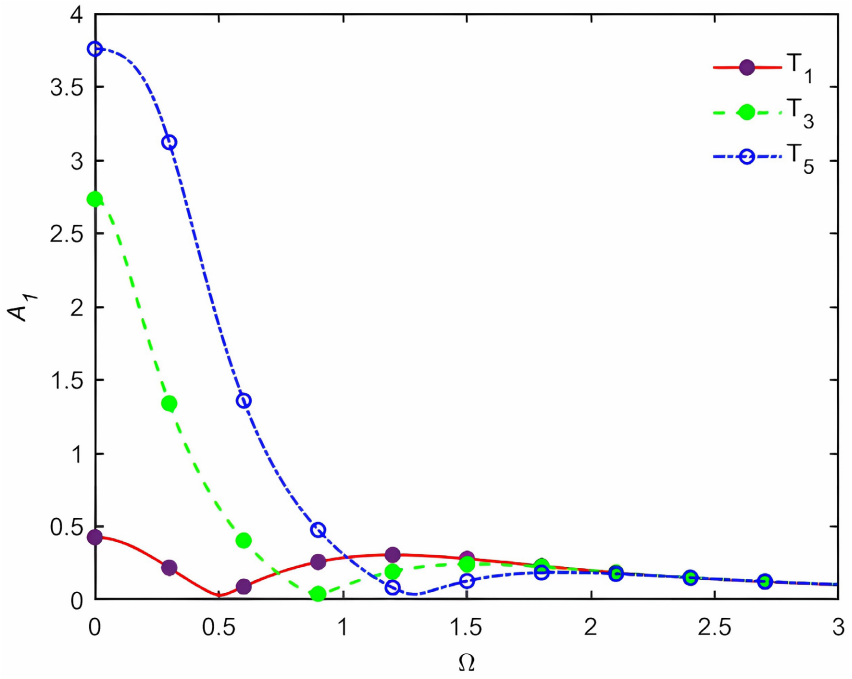

Figure 15. The amplitude-frequency response curves corresponding to the three points of T_1, T_3, T_5 .

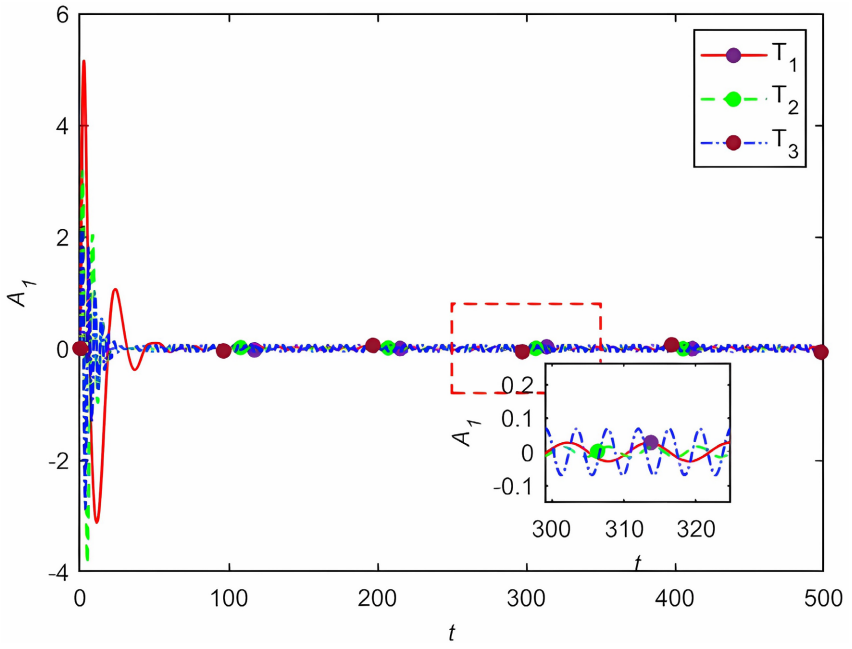

Figure 16. The time history curves corresponding to the three points of T_1, T_3, T_5 .

Substitute g and τ corresponding to the three points of T_1, T_3, T_5, as well as the optimal structural parameters D_4 into the amplitude Equation (11), and draw the amplitude-frequency response curves corresponding to these three

points as shown in Figure 15. It can be seen from the figure that the anti-resonance amplitudes corresponding to the three measuring points all meet the requirements of the anti-resonance optimization criterion (that is $A_1 < 10^{-1}$), and their corresponding anti-resonance frequencies are the same as the values in Figure 13.

Finally, a time-domain verification is carried out for the three points of T_1, T_3, T_5. The anti-resonance frequencies Ω_a corresponding to these three measuring points are selected as the external excitation frequencies. After substituting the known parameters into the dimensionless Equation (3-3), the dde23 function in Matlab is used to solve Equation (3). The time t = 500S is selected, and the time history curves of the three measuring points are drawn as shown in Figure 16. It can be found from the figure that the amplitudes of the three measuring points gradually decrease and converge over time, indicating that the system tends to be stable. From the locally enlarged view, it can be found that the amplitudes of the three measuring points are all within 0.1, which meets the conditions set by the optimization criterion.

4.3. Comparison of Vibration Reduction Effects of Different Vibration Absorber Models

In order to further analyze the excellent vibration reduction performance of the dynamic vibration absorber with time-delay feedback control, the optimized results are quantitatively compared with the vibration reduction effects of the other two types of dynamic vibration absorbers. Taking the measuring point T_1 as an example for the optimization results in this paper, the structural parameters used are represented by D_4, and the optimal parameters of Xing and Yang are represented by P_X and P_Y respectively. The parameters are shown in Table 2, and the amplitude-frequency response curves of the three different dynamic vibration absorbers are drawn as shown in Figure 17.

Table 2. Comparison of optimal structural parameters.

Structural parameters	Xing	Yang	D_4
μ	0.100	0.100	0.100
ξ_1	0	0	0.4797
ξ_2	0.5415	1.0279	1.0279
p	0.6931	0.7302	0.7302
β	0	0.800	1.0222
α	−0.5592	8.9230	−1.4444
L	2.5	2.5	2.5

It can be seen from Figure 17 that when the external excitation frequency is within 3, the time-delay negative stiffness dynamic vibration absorber with an inerter designed in this chapter has achieved a very good vibration reduction effect.

Compared with Xing's vibration absorber model, it has significantly broadened the vibration reduction frequency band. When compared with Yang's vibration absorber model, it has excellent vibration reduction characteristics throughout the entire frequency range. Moreover, at the anti-resonance point, the dynamic vibration absorber designed in this paper can almost completely absorb the vibration. This can effectively prevent the main system from generating large-amplitude vibrations at specific frequencies, ensuring its operational stability and safety, and preventing problems such as structural damage and performance degradation caused by resonance.

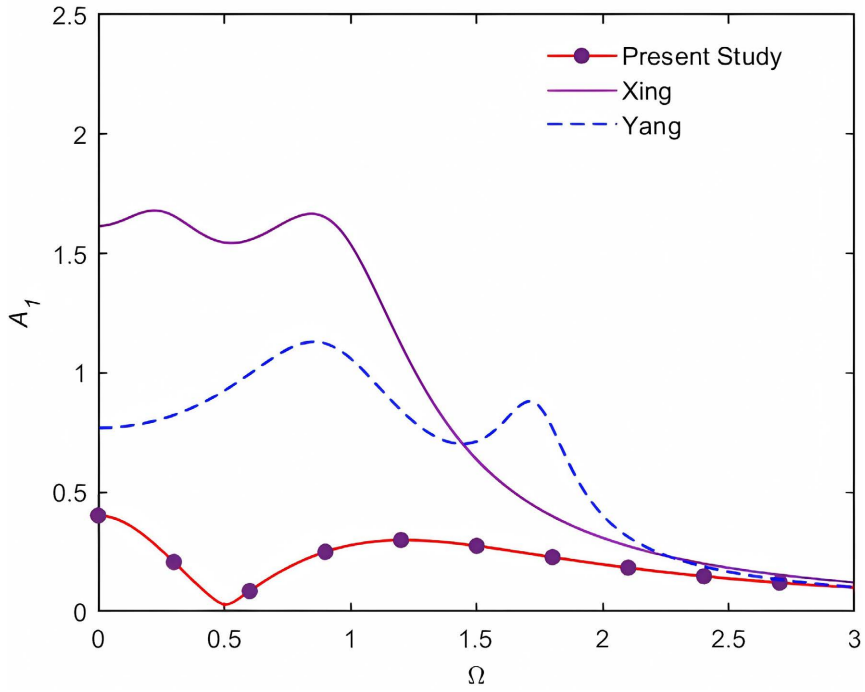

Figure 17. Comparison of the amplitude-frequency response curves of different vibration absorber models.

5. Conclusions

The model proposed in this paper combines the dual advantages of negative stiffness and amplifying mechanism, which not only has excellent performance in vibration reduction effect, but also needs to be applied to practice in engineering implementation in combination with precision mechanical design and active control technology. In the future, it is expected to reduce the vibration of dynamic vibration absorbers combined with negative stiffness and amplifying mechanisms in ships, machinery, construction, transportation and other fields. According to the above research, the following conclusions can be drawn:

1) When the time-delay feedback control is not considered, the optimal parameter expression of the system under passive control is obtained by using the H_∞ optimization criterion, and the optimal working range of the inerter is calculated. Within this range, the DVA has a good vibration reduction effect.

2) When the time-delay feedback control exists, the characteristic equation of the system is a transcendental equation containing exponential terms. The stability analysis of the system is carried out through the CTCR method and the Dxion resultant, and the corresponding optimization criterion for the anti-resonance peak is designed.

3) As the negative stiffness coefficient α continuously increases, the stable intervals of the feedback gain coefficient g and the time-delay quantity τ also keep expanding. Under the condition of meeting the optimization criterion for the anti-resonance point, there exists an optimal negative stiffness value that can make the anti-resonance frequency band width the widest while maintaining good symmetry.

4) As the damping ξ_1 of the main system continuously increases, the stable intervals of g and τ keep expanding, and the width of the adjustable anti-resonance frequency first decreases and then increases. Under this condition, there exists an optimal damping ξ_1 of the main system, which can make the adjustable anti-resonance point frequency band have good symmetry with respect to the main resonance point, and at the same time, ensure that the adjustable anti-resonance point frequency band has a certain width.

5) Within the optimal working interval of the inerter ratio β, as the inerter ratio continuously increases, the stable intervals of g and τ gradually decrease, while the width of the adjustable anti-resonance frequency first decreases and then increases. Under this condition, there exists an optimal inerter ratio β that enables the adjustable anti-resonance point frequency band to have good symmetry with respect to the main resonance point and at the same time ensures the bandwidth of the anti-resonance point frequency band.

6) Within the stable interval of the system, there exists a set of optimal values for the feedback gain coefficient and the time-delay quantity. At the anti-resonance point, compared with the vibration absorber models of Xing and Yang, the dynamic vibration absorber designed in this paper can greatly absorb and dissipate the vibration energy of the main system.

7) Through the innovative combination of negative stiffness elements and amplifying mechanism, the dynamic vibration absorber model significantly broadens the damping frequency band in theory, and provides theoretical support and design basis for the dynamic vibration absorber combined with negative stiffness and amplifying mechanism.

Funding

This work was supported by the National Natural Science Foundation of China (12072140).

Conflicts of Interest

The authors declare no conflicts of interest regarding the publication of this paper.

References

[1] Frahm, A. (1909) Device for Damping Vibrations of Bodies. US Patent 989958.

[2] Ormondroyd, J. and Den Hartog, J.P. (1928) The Theory of the Dynamic Vibration Absorber. *Transactions of the American Society of Mechanical Engineers*, **49**, Article ID: 021007. https://doi.org/10.1115/1.4058553

[3] Den Hartog, J.P. (1974) Mechanical Vibrations. McGraw-Hill Book Company.

[4] Den Hartog, J.P. (1985) Mechanical Vibrations. Dover Publications.

[5] Brock, J.E. (1946) A Note on the Damped Vibration Absorber. *Journal of Applied Mechanics*, **13**, A284. https://doi.org/10.1115/1.4009588

[6] Nishihara, O. and Asami, T. (2002) Closed-Form Solutions to the Exact Optimizations of Dynamic Vibration Absorbers (Minimizations of the Maximum Amplitude Magnification Factors). *Journal of Vibration and Acoustics*, **124**, 576-582. https://doi.org/10.1115/1.1500335

[7] Asami, T. and Nishihara, O. (2003) Closed-Form Exact Solution to H_∞ Optimization of Dynamic Vibration Absorbers (Application to Different Transfer Functions and Damping Systems). *Journal of Vibration and Acoustics*, **125**, 398-405. https://doi.org/10.1115/1.1569514

[8] Liu, L.L., Ren, B.L. and Zhu, G.D. (2017) Research on Dynamic Characteristics of Bistable Electromagnetic Vibration Absorber Considering Nonlinear Damping. *Journal of Vibration and Shock*, **36**, 91-96. https://doi.org/10.13465/j.cnki.jvs.2017.17.015

[9] Zhao, Y.Y. and Xu, J. (2008) Damping Mechanism of Time-Delayed Nonlinear Dynamic Vibration Absorber. *Chinese Journal of Theoretical and Applied Mechanics*, **40**, 98-106. https://doi.org/10.6052/0459-1879-2008-1-2007-078

[10] Zhao, Y.Y. and Xu, J. (2011) Vibration Control of Self-Parameter Vibrating Systems Using Time-Delayed Feedback. *Chinese Journal of Theoretical and Applied Mechanics*, **43**, 894-904. https://doi.org/10.6052/0459-1879-2011-5-lxxb2010-652

[11] Peng, H.B., Shen, Y.J. and Yang, S.P. (2015) Parameter Optimization of a Novel Dynamic Vibration Absorber with Negative Stiffness Components. *Chinese Journal of Theoretical and Applied Mechanics*, **47**, 320-327. https://doi.org/10.6052/0459-1879-14-275

[12] Oyelade, A.O., Wang, Z. and Hu, G. (2017) Dynamics of 1D Mass-Spring System with a Negative Stiffness Spring Realized by Magnets: Theoretical and Experimental Study. *Theoretical and Applied Mechanics Letters*, **7**, 17-21. https://doi.org/10.1016/j.taml.2016.12.004

[13] Yi, J., Xu, K. and He, X.H. (2024) Parameter Optimization and Seismic Response Control of Tuned Negative Stiffness-Inertial Mass Damping System. *Journal of Vibration Engineering*, **37**, 1015-1022. https://doi.org/10.16385/j.cnki.issn.1004-4523.2024.06.012

[14] Gao, H., Xing, C.X. and Wang, H. (2023) Enhancement of Seismic Performance of Isolated Structures Using Tuned Negative Stiffness-Inertial Mass Dampers. *Journal of Southeast University* (*Natural Science Edition*), **53**, 592-599. https://doi.org/10.3969/j.issn.1001-0505.2023.04.004

[15] Wang, J., Zhang, Y. and Huang, S. (2023) Analytical Study on Parameter Optimization of Inertial-Mass Damping Systems with Negative Stiffness under Displacement Excitation. *Journal of Vibration Engineering*, **36**, 804-814. https://doi.org/10.16385/j.cnki.issn.1004-4523.2023.03.023

[16] Zhang, Y., Liu, G.L. and Zhou, P. (2024) Study on the Vibration Reduction Effect of

Cable Systems with Negative Stiffness Dampers under Flexible Supports. *Highway*, No, 5, 142-146.

[17] Tu, L., Ning, D., Sun, S., Li, W., Huang, H., Dong, M., *et al.* (2020) A Novel Negative Stiffness Magnetic Spring Design for Vehicle Seat Suspension System. *Mechatronics*, **68**, Article ID: 102370. https://doi.org/10.1016/j.mechatronics.2020.102370

[18] Benacchio, S., Malher, A., Boisson, J. and Touzé, C. (2016) Design of a Magnetic Vibration Absorber with Tunable Stiffnesses. *Nonlinear Dynamics*, **85**, 893-911. https://doi.org/10.1007/s11071-016-2731-3

[19] Hu, F.Y., Liu, Q.H. and Cao, J.Y. (2021) Parameter Identification Method for the Restoring Force Surface of Negative Stiffness Nonlinear Systems. *Journal of Xi'an Jiaotong University*, **55**, 95-106.https://doi.org/10.7652/xjtuxb202104011

[20] Zang, J., Yuan, T., Lu, Z., Zhang, Y., Ding, H. and Chen, L. (2018) A Lever-Type Nonlinear Energy Sink. *Journal of Sound and Vibration*, **437**, 119-134. https://doi.org/10.1016/j.jsv.2018.08.058

[21] Yang, W.Q., Hua, X.G. and Wen, Q. (2021) Vibration Reduction Optimization of Lever-Type Tuned Mass Dampers for Vortex-Induced Vibrations of Twin Cable Suspensions. *Journal of Vibration Engineering*, **34**, 819-827. https://doi.org/10.16385/j.cnki.issn.1004-4523.2021.04.019

[22] Xu, X.M., Fu, M.H. and Li, J.X. (2016) Study on a Novel Lever-Type Variable Friction Damper for Heavy-Duty Truck Bogies. *Mechanical Engineering and Automation*, No. 6, 18-20. https://doi.org/10.3969/j.issn.1672-6413.2016.06.008

[23] Li, C.X. and Xiong, X.Y. (2003) Dynamic Characteristics of a New Model Strategy for Lever-Type Tuned Mass Damper (LT-TMD). *Sichuan Building Science*, No. 4, 73-75.

[24] Wang, X., He, T., Shen, Y., Shan, Y. and Liu, X. (2019) Parameters Optimization and Performance Evaluation for the Novel Inerter-Based Dynamic Vibration Absorbers with Negative Stiffness. *Journal of Sound and Vibration*, **463**, Article ID: 114941. https://doi.org/10.1016/j.jsv.2019.114941

[25] Yang, X.T., Shen, Y.J. and Wang, J.F. (2022) Parameter Optimization of a Dynamic Vibration Absorber with an Amplification Mechanism, Inerter and Grounded Stiffness. *Journal of Vibration and Shock*, **41**, 308-315. https://doi.org/10.13465/j.cnki.jvs.2022.21.035

[26] Sipahi, R. and Olgac, N. (2006) Stability Robustness of Retarded LTI Systems with Single Delay and Exhaustive Determination of Their Imaginary Spectra. *SIAM Journal on Control and Optimization*, **45**, 1680-1696. https://doi.org/10.1137/050633238